Cellular and Molecular Life Sciences (2018) 75:4445–4464
https://doi.org/10.1007/s00018-018-2890-0

Cellular and Molecular Life Sciences

ORIGINAL ARTICLE

PTEN–GSK3β–MOB1 axis controls neurite outgrowth in vitro and in vivo

Zhiwen Song[1] · Xiu Han[2] · Hongjun Zou[1] · Bin Zhang[3] · Ya Ding[1] · Xu Xu[1] · Jian Zeng[2] · Jinbo Liu[1] · Aihua Gong[2]

Received: 21 November 2017 / Revised: 23 July 2018 / Accepted: 25 July 2018 / Published online: 1 August 2018

Abstract

Mps One binder 1 (MOB1) is a core component of NDR/LATS kinase and a positive regulator of the Hippo signaling pathway. However, its role in neurite outgrowth still remains to be clarified. Here, we confirmed, for the first time, that MOB1 promoted neurite outgrowth and was involved in functional recovery after spinal cord injury (SCI) in mice. Mechanistically, we found that MOB1 stability was regulated by the PTEN–GSK3β axis. The MOB1 protein was significantly up-regulated in PTEN-knockdown neuronal cells. This effect was dependent on the lipid phosphatase activity of PTEN. Moreover, MOB1 was found to be a novel substrate for GSK3β that is phosphorylated on serine 146 and degraded via the ubiquitin–proteasome system (UPS). Finally, in vivo lentiviral-mediated silencing of PTEN promoted neurite outgrowth and functional recovery after SCI and this effect was reversed by down-regulation of MOB1. Taken together, this study provided mechanistic insight into how MOB1 acts as a novel and a necessary regulator in PTEN–GSK3β axis that controls neurite outgrowth after SCI.

Keywords MOB1 · PTEN · GSK3β · Neurite outgrowth · Spinal cord injury

Introduction

Functional recovery following SCI is limited by multiple developmentally related and injury-induced mechanisms that restrict axonal regeneration in the adult central nervous system (CNS) [1, 2]. The injury-disturbed environment affects several intracellular signaling pathways including PTEN/mTOR, Jak/STAT, DLK/JNK, which destabilize the microtubule cytoskeleton and growth cone structures and eventually leads to neurite outgrowth inhibition [3, 4]. Therefore, regulation of neurite outgrowth is important for developing therapies that enhance the repair of injured neurons after SCI.

MOB1 was initially identified as a yeast gene required for the completion of mitosis and maintenance of ploidy [5]. In mammalian cells, MOB1 is required for efficient centrosome duplication, the major microtubule organizing center [6, 7]. Depletion of MOB1 causes abscission failure as a consequence of hyper-stabilization of microtubules in the midbody region [8], suggesting that MOB1 is involved in microtubule stability. In addition, MOB1 protein has been shown to bind and activate nuclear Dbf2-related (NDR) kinase, a subfamily of serine/threonine protein kinases that control cell division and morphogenesis in various cell types including neuronal cells [9–11]. NDR1/2 double knockdown prevents the formation of supernumerary axons during the polarization of hippocampal neurons [11] and NDR2 overexpression enhances neurite outgrowth in mouse primary cultured neurons [12], indicating that MOB1 and NDR1/2 are involved in the regulation of neurite outgrowth in mammalian CNS. Interestingly, Lin et al. found that Mps One binder 2 (MOB2), not MOB1, significantly promoted neurite formation by binding to NDR2 in vitro [13]. However, our preliminary studies revealed that MOB1 played a role in neurite outgrowth in vivo and in vitro. In this study, we will

Electronic supplementary material The online version of this article (https://doi.org/10.1007/s00018-018-2890-0) contains supplementary material, which is available to authorized users.

✉ Jinbo Liu
czljbljb@126.com

✉ Aihua Gong
ahg5@mail.ujs.edu.cn

[1] Department of Orthopaedics, School of Medicine, The Third Affiliated Hospital of Soochow University, Changzhou 213000, China

[2] Department of Cell Biology, School of Medicine, Jiangsu University, Zhenjiang 212013, China

[3] Department of Laboratory Medicine, Affiliated Hospital of Jining Medical University, Jining 272000, China

clarify the roles and mechanisms of MOB1 in promoting neurite outgrowth and functional recovery after CNS injury.

Phosphatase and tensin homologue (PTEN) is an important negative regulator of the evolutionarily conserved PI3K pathway that regulates neuronal survival, axonal regrowth and functional recovery after adult CNS injury [14–16]. Previous studies have shown that PI3K signaling recruits Akt to the plasma membrane to be activated by phosphorylation at T308 via phosphoinositide-dependent kinase-1 (PDK1) [17, 18]. Phosphorylated Akt in turn phosphorylates glycogen synthase kinase3β (GSK3β) at Ser9 residue and inhibits its activity [19], which is critical to regulating neuronal polarization, axonal microtubule assembly and neurite outgrowth in mammalian CNS [18, 20, 21]. Currently, the effect of GSK3β on nerve regeneration is controversial, some studies suggest that suppression of GSK3β activity is required for the neurite outgrowth [22] and axonal elongation [23, 24], while others show that GSK3β significantly promotes axon extension [25, 26]. It is likely that GSK3β is a serine/threonine kinase that phosphorylates different nerve-associated proteins, activating or degrading them in many different pathways. One known example is that GSK3β phosphorylates and activates serum response factor (SRF) to promote axonal outgrowth in mouse hippocampal neurons [25]. However, the role of PTEN–GSK3β axis in neurite outgrowth and its downstream molecular targets are poorly characterized.

In this study, we demonstrated that MOB1 promoted neurite outgrowth and was involved in functional recovery after SCI in mice, which was required for PTEN–GSK3β axis. Importantly, we showed that the lipid phosphatase activity of PTEN modulated the MOB1 protein stability by activating GSK3β which bound and phosphorylated MOB1 at the Ser146 and degraded ubiquitylated MOB1 via the UPS. It is suggested that PTEN–GSK3β–MOB1 axis may be a potential therapeutic approach to improve functional recovery after SCI.

Results

Expression profiles of PTEN and MOB1 during the development of mouse CNS, in Muridae cells, and after SCI

In the mammalian CNS, PTEN is essential for embryonic development [27]. MOB1 protein is a key regulator of large tumor suppressor 1/2 (LATS1/2) kinases in the Hippo pathway, which regulates cell numbers and organ size in multicellular organisms [28, 29]. Here we aimed to determine the involvement of MOB1 in CNS development. First, we examined the expression of PTEN and MOB1 protein in mice brain (hippocampus) and spinal cord from embryonic stage 15 days to adult by western blot (Fig. 1a, c). We found that the expression of MOB1 was high during the gestation period, especially in the spinal cord. However, its expression gradually and stably decreased 7 days after birth. Interestingly, this phenomenon was negatively correlated with the protein expression of PTEN (Fig. 1b, d). These results suggested a relationship between PTEN and MOB1 in the CNS. Similarly, we analyzed the expression of PTEN and MOB1 in multiple Muridae cell lines using western blot. As shown in Fig. 1e, f, the protein expression of PTEN and MOB1 was negatively correlated. Finally, we checked the protein levels of MOB1 and PTEN after injury by western blot. We found that the expression level of PTEN increased significantly at 1 week after injury, and gradually decreased afterwards. Consistently, there was a negative relationship between the expression of MOB1 and PTEN (Fig. 1g, h).

PTEN–MOB1 axis controls neurite outgrowth in vitro

To further test the association of PTEN with MOB1, we constructed three independent PTEN-shRNAs plasmids and sh-EGFP as a control. After transfection, the protein levels of MOB1 significantly increased in the three sh-PTEN groups (Fig. 2a, b). But, the mRNA level of MOB1 did not change in all three groups (Fig. 2c). To confirm these results, we used mouse neuroblastoma Neuro2A and rat pheochromocytoma PC12 cell lines as in vitro research models to investigate neurite outgrowth [30, 31]. First, we generated stable cell lines: PC12-sh-PTEN, PC12-sh-EGFP, Neuro2A-sh-PTEN and Neuro2A-sh-EGFP. We then found that PTEN knockdown significantly up-regulated MOB1 protein expression compared to the control group (Fig. 2d–f), but it had no effect on mRNA levels of MOB1 (Fig. 2j, k). Using the phase contrast microscope, higher neurite formation was observed in PC12-sh-PTEN (122.1 ± 2.3 μm) and Neuro2A-sh-PTEN (126.3 ± 1.9 μm) cells compared to PC12-sh-EGFP (20.7 ± 2.8 μm) and Neuro2A-sh-EGFP (18.7 ± 3.2 μm) cells, respectively (Fig. 2g–i). Subsequently, we examined the effects of PTEN on neurite outgrowth by detecting the expression of growth-associated protein 43 (GAP43) and neurofilament 200 (NF200), which have been reported to play a role in neurite outgrowth [32, 33]. We observed a significant increase in GAP43, p-GAP43 (S41) and NF200 proteins in PC12-sh-PTEN and Neuro2A-sh-PTEN cells (Fig. 2d–f).

To determine whether the MOB1 affects neurite outgrowth, we used two highly conserved variants of MOB1, MOB1A and MOB1B. Two plasmids were constructed, Flag-MOB1A and Flag-MOB1B plasmids, and a vector as a control. As shown in Fig. 1e, the expression of MOB1 was relatively lower in PC12 cells compared with other mice cells and the amino acid sequences of MOB1 in rat and murine were similar. Therefore, overexpression of

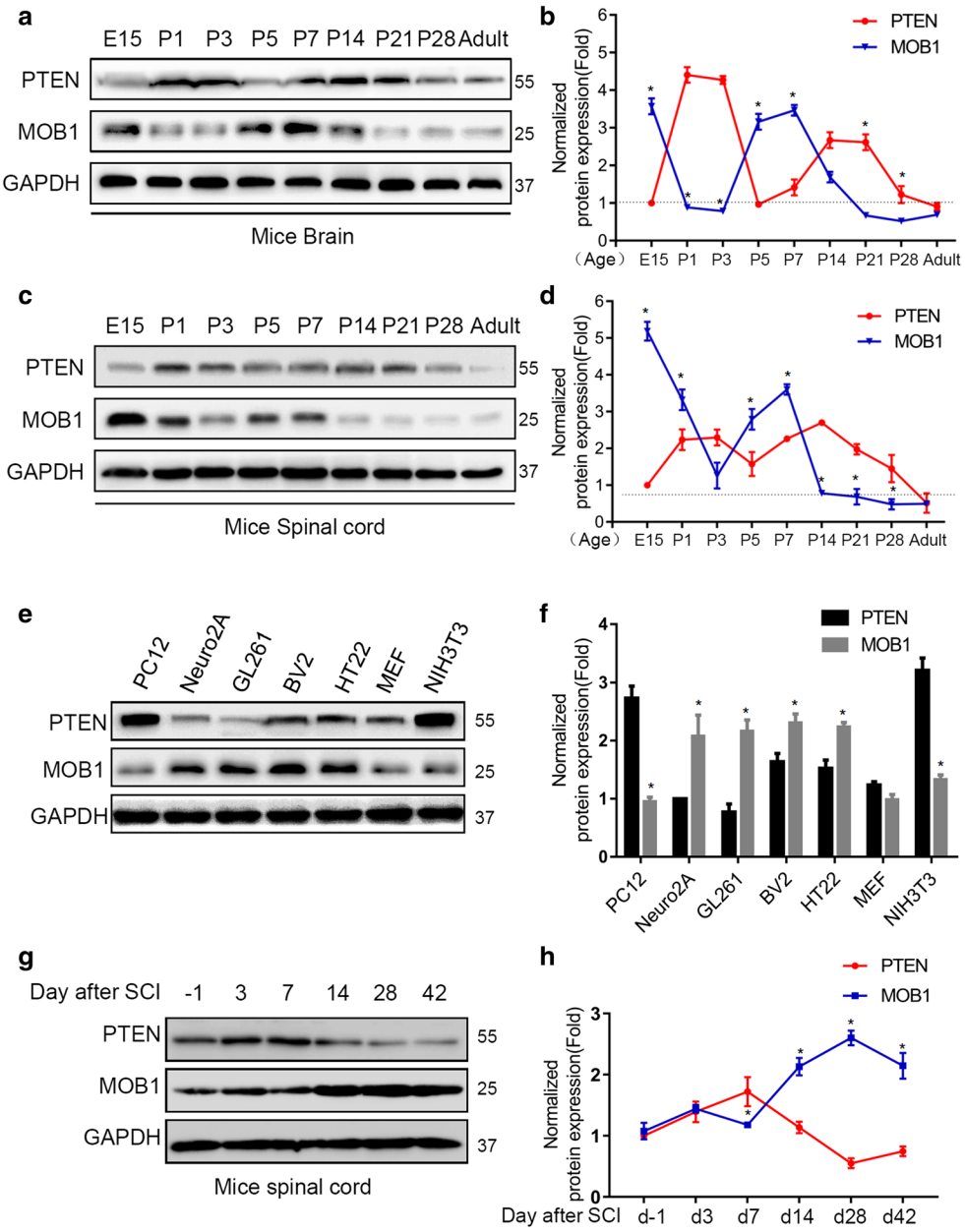

Fig. 1 Expression profiles of PTEN and MOB1 during the development of mice brain and spinal cord and in Muridae cell lines. Western blot analysis showing relative expression of PTEN and MOB1 from embryonic stage 15 days to adult in mice brain (hippocampus) (**a**, **b**) and spinal cord (**c**, **d**), and GAPDH served as an internal control (*$P < 0.05$ vs. PTEN at each time point, two-way ANOVA followed by *t* test). **e**, **f** The PTEN and MOB1 expression at the protein level in seven types of Muridae cells and GAPDH served as an internal control (*$P < 0.05$ vs. PTEN, *t* test). **g**, **h** Western blot analysis showing relative expression of PTEN and MOB1 upon SCI and GAPDH served as an internal control (*$P < 0.05$ vs. PTEN at each time point, two-way ANOVA followed by *t* test)

Flag-MOB1A or Flag-MOB1B was sufficient to increase GAP43 and NF200 at mRNA and protein levels, respectively (Fig. 2l–m). In addition, immunostaining results were consistent with those described above, which indicated that MOB1 functions as a neurite outgrowth-promoting molecule after nerve injury (Fig. 2o, p).

To test whether down-regulation of PTEN enhances neurite outgrowth in a MOB1-dependent manner. We used two shRNAs against MOB1A and MOB1B in PC12-sh-PTEN cells to evaluate neurite outgrowth (Fig. 3a–d). The results indicated that MOB1 was required for neurite outgrowth induced by PTEN knockdown. However, we found that the PTEN-induced MOB1 degradation did not affect the phosphorylation of YAP or its nuclear translocation in vitro (Fig. 3e–h).

To confirm the results above, we cultured primary hippocampal neurons from mouse hippocampus (Figure S1a). The effects of PTEN on MOB1 expression and its influence on neurite outgrowth were detected by western blot and immunofluorescence staining. After infection of primary hippocampal neurons with Lenti-sh-PTEN, the results showed that the length of the neurites was increased compared with the Lenti-control group. PTEN knockdown increased the expression of MOB1, p-GSK3β and neurite outgrowth markers (NF200, GAP43 and p-GAP43) (Figure S1b–e). Moreover, MOB1A overexpression increased the

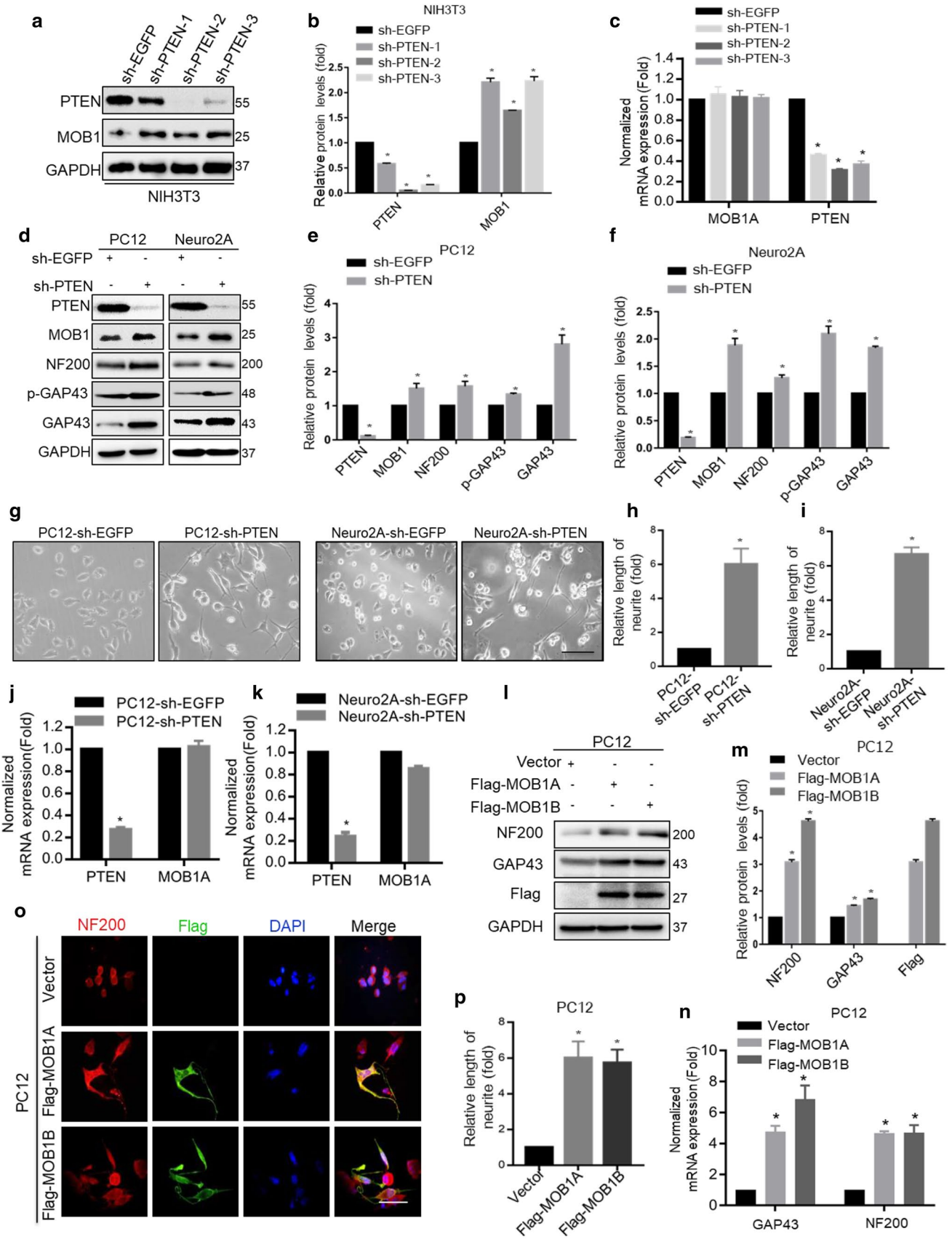
a
sh-EGFP
sh-PTEN-1
sh-PTEN-2
sh-PTEN-3
PTEN
MOB1
GAPDH
55
25
37
NIH3T3
b
NIH3T3
sh-EGFP
sh-PTEN-1
sh-PTEN-2
sh-PTEN-3
Relative protein levels (fold)
PTEN
MOB1
c
sh-EGFP
sh-PTEN-1
sh-PTEN-2
sh-PTEN-3
Normalized mRNA expression (Fold)
MOB1A
PTEN
d
PC12
Neuro2A
sh-EGFP
sh-PTEN
PTEN
MOB1
NF200
p-GAP43
GAP43
GAPDH
55
25
200
48
43
37
e
PC12
sh-EGFP
sh-PTEN
Relative protein levels (fold)
PTEN
MOB1
NF200
p-GAP43
GAP43
f
Neuro2A
sh-EGFP
sh-PTEN
Relative protein levels (fold)
PTEN
MOB1
NF200
p-GAP43
GAP43
g
PC12-sh-EGFP
PC12-sh-PTEN
Neuro2A-sh-EGFP
Neuro2A-sh-PTEN
h
Relative length of neurite (fold)
PC12-sh-EGFP
PC12-sh-PTEN
i
Relative length of neurite (fold)
Neuro2A-sh-EGFP
Neuro2A-sh-PTEN
j
PC12-sh-EGFP
PC12-sh-PTEN
Normalized mRNA expression(Fold)
PTEN
MOB1A
k
Neuro2A-sh-EGFP
Neuro2A-sh-PTEN
Normalized mRNA expression(Fold)
PTEN
MOB1A
l
PC12
Vector
Flag-MOB1A
Flag-MOB1B
NF200
GAP43
Flag
GAPDH
200
43
27
37
m
PC12
Vector
Flag-MOB1A
Flag-MOB1B
Relative protein levels (fold)
NF200
GAP43
Flag
o
NF200
Flag
DAPI
Merge
PC12
Vector
Flag-MOB1A
Flag-MOB1B
p
PC12
Relative length of neurite (fold)
Vector
Flag-MOB1A
Flag-MOB1B
n
PC12
Vector
Flag-MOB1A
Flag-MOB1B
Normalized mRNA expression (Fold)
GAP43
NF200

◂**Fig. 2** PTEN knockdown up-regulates MOB1 expression to promote neurite outgrowth by activating the PI3K/Akt signaling pathway in vitro. The changes in PTEN and MOB1 protein (**a**, **b**) and mRNA (**c**) levels were detected using western blot and real-time PCR analysis in NIH3T3 cells transfected with three independent PTEN-shRNAs: sh-PTEN-1, sh-PTEN-2 and sh-PTEN-3, or sh-EGFP plasmids. GAPDH was used as an internal control (*$P < 0.05$, ANOVA test). **d–f** PTEN, MOB1, GAP43, p-GAP43, and NF200 protein levels were measured using western blotting in stable PC12 and Neuro2A cells with PTEN knockdown, and GAPDH served as an internal control (*$P < 0.05$, *t* test). **g** Morphological changes were photographed using a digital CCD camera. Both the length of neurite and the number of neurite-presenting cells increased in stable PC12 and Neuro2A cells with PTEN knockdown. Scale bar, 150 μm. The quantification of the neurite length in PC12 cells (**h**) and Neuro2A cells (**i**) (*$P < 0.05$, *t* test). PTEN knockdown had no effect on mRNA levels of MOB1 expression in PC12 (**j**) and Neuro2A (**k**) cells (*$P < 0.05$, *t* test). Overexpression of Flag-MOB1A or Flag-MOB1B was sufficient to increase GAP43 and NF200 at the protein (**l**, **m**) and mRNA (**n**) levels in PC12 cells, respectively. GAPDH served as an internal control (*$P < 0.05$, ANOVA test). **o** Representative immunofluorescence images with anti-NF200 and anti-Flag in PC12 cells transfected with Flag-MOB1A, Flag-MOB1B or Vector. Scale bar, 100 μm. **p** The quantification of the neurite length in PC12 cells (*$P < 0.05$, ANOVA test)

length of neurite and expression of neurite outgrowth markers in primary hippocampal neurons (Figure S1f–j).

Lipid phosphatase activity of PTEN regulates MOB1 protein level in vitro

It was previously reported that PTEN is a tumor suppressor molecule with phosphatase activity against lipids and proteins and possesses other non-enzymatic mechanisms of action [34]. To explore the mechanism of PTEN in the regulation of MOB1, we constructed Flag-PTEN (wild type, WT) or mutant PTEN-harboring a loss-of-function mutation in the protein (Y138L) [35], lipid (G129E) [36], or phosphatase domain (C124S) [37]. First, we performed IP assays to evaluate whether PTEN physically interacts with MOB1. The result showed that the two proteins did not have direct interaction (Fig. 4a). Next, we transfected the WT or mutant PTEN constructs into Neuro2A cells. Surprisingly, both PTEN WT and the Y138L protein phosphatase mutant remarkably reduced the endogenous expression of MOB1 and increased the expression of phosphorylated GSK3β-S9 (Fig. 4b, c). No significant differences were observed between the expression of MOB1 and p-GSK3β-S9 in Neuro2A cells transfected with vector control, G129E, or C124S constructs. These series of experiments demonstrated that the lipid phosphatase activity of PTEN had effects on MOB1.

Further experiments were performed to confirm this result and to identify the downstream targets of the PTEN-PI3K signaling that directly modulate MOB1 expression. We first found that knockdown of PTEN significantly increased p-PDK1-S241, p-Akt-T308, p-GSK3β-S9 and MOB1 expression (Fig. 4d–f). We then used three specific pharmacologic inhibitors of PTEN-PI3K downstream pathways to explore the mechanism by which PTEN affected the protein expression of MOB1. PC12-sh-PTEN and Neuro2A-sh-PTEN cells were treated with PI3K inhibitor LY294002 [38] or DMSO as a control. We observed that LY294002 could rescue the MOB1 stability and block the phosphorylation of PDK1, Akt and GSK3β induced by PTEN knockdown (Fig. 4d–f). BX795 [39], an inhibitor of the PI3K downstream effector PDK1, blocked the effect of PTEN on MOB1 compared to DMSO control group (Fig. 4g–i). Previous studies indicated that PDK1 selectively phosphorylates T308 of Akt which is the major downstream kinase of the PI3K pathway [39]. In addition, we showed that Perifosine [40], a novel Akt inhibitor, also decreased MOB1 expression and the level of p-GSK3β-S9 in PC12-sh-PTEN and Neuro2A-sh-PTEN cells compared to DMSO control group (Fig. 4j–l). Collectively, these data showed that the absence of PTEN increased MOB1 expression which promoted neurite outgrowth by activating the PI3K/PDK1/Akt/GSK3β signaling pathway, suggesting that GSK3β may directly regulate MOB1 protein expression.

GSK3β kinase regulates the stability of the MOB1 protein

Since GSK3β phosphorylates a broad range of substrates including APC [41], Cdc25A [42], and FoxM1 [43], thereby marking them for degradation via the proteasome, we explored whether GSK3β also modulates MOB1 degradation. PC12 cells were treated with a GSK3β inhibitor, LiCl, in addition to a protein synthesis inhibitor, CHX. LiCl stabilized MOB1 protein in the presence of CHX (Fig. 5a, c). Subsequently, PC12-sh-PTEN cells were treated with CHX at the indicated time points (0, 2, 4 and 6 h). PTEN knockdown significantly increased the half-life of MOB1 through elevated GSK3β activity (Fig. 5b, d). To confirm that GSK3β regulates MOB1 stability, we measured the MOB1 protein degradation in GSK3β$^{+/+}$ and GSK3β$^{-/-}$ mouse embryonic fibroblast (MEF) cells in the presence of CHX. We found that MOB1 expression was considerably stable in MEF GSK3β$^{-/-}$ cells over time (Fig. 5e, f). To determine whether GSK3β kinase activity affects MOB1 protein stability, the MOB1 levels were monitored in HEK293T cells overexpressing constitutively active (CA) or kinase-inactive (KD) GSK3β (corresponding to the sequence of the human GSK3β protein). As shown in Fig. 5g, h, MOB1 protein levels were reduced in GSK3β-CA group relative to GSK3β-KD group.

We further tested whether PTEN regulates MOB1 stability via GSK3β. The results showed that PTEN knockdown could not increase MOB1 expression in MEF GSK3β$^{-/-}$ cells

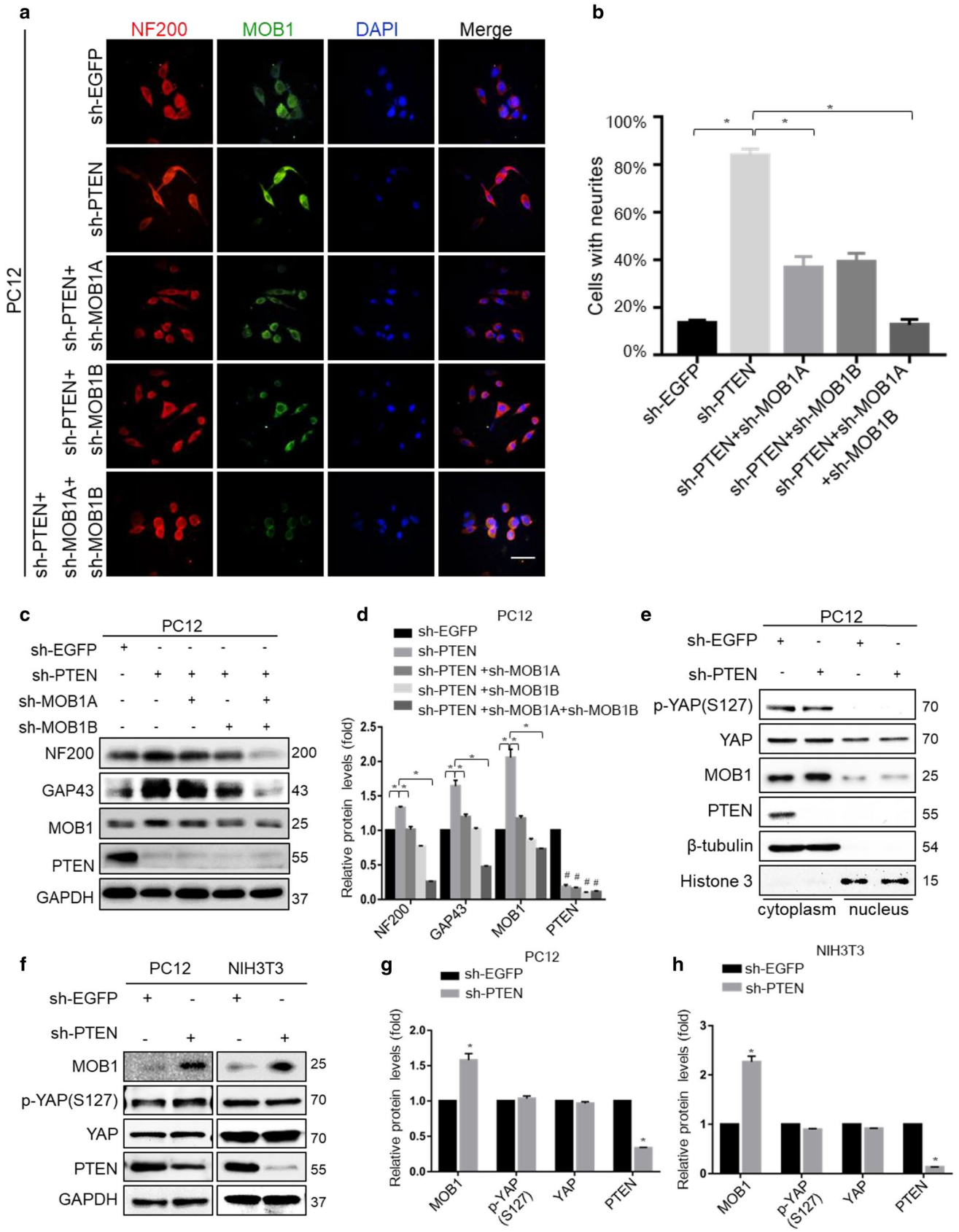
a
NF200
MOB1
DAPI
Merge
PC12
sh-EGFP
sh-PTEN
sh-PTEN+ sh-MOB1A
sh-PTEN+ sh-MOB1B
sh-PTEN+ sh-MOB1A+ sh-MOB1B
b
Cells with neurites
100%
80%
60%
40%
20%
0%
sh-EGFP
sh-PTEN
sh-PTEN+sh-MOB1A
sh-PTEN+sh-MOB1B
sh-PTEN+sh-MOB1A +sh-MOB1B
c
PC12
sh-EGFP
sh-PTEN
sh-MOB1A
sh-MOB1B
NF200
GAP43
MOB1
PTEN
GAPDH
200
43
25
55
37
d
PC12
sh-EGFP
sh-PTEN
sh-PTEN +sh-MOB1A
sh-PTEN +sh-MOB1B
sh-PTEN +sh-MOB1A+sh-MOB1B
Relative protein levels (fold)
NF200
GAP43
MOB1
PTEN
e
PC12
sh-EGFP
sh-PTEN
p-YAP(S127)
YAP
MOB1
PTEN
β-tubulin
Histone 3
70
70
25
55
54
15
cytoplasm
nucleus
f
PC12
NIH3T3
sh-EGFP
sh-PTEN
MOB1
p-YAP(S127)
YAP
PTEN
GAPDH
25
70
70
55
37
g
PC12
sh-EGFP
sh-PTEN
Relative protein levels (fold)
MOB1
p-YAP (S127)
YAP
PTEN
h
NIH3T3
sh-EGFP
sh-PTEN
Relative protein levels (fold)
MOB1
p-YAP (S127)
YAP
PTEN

◂**Fig. 3** MOB1 suppression abolishes the neurite outgrowth in PTEN knockdown cells, which is independent of phosphorylation of YAP and YAP nuclear translocation. Representative immunofluorescence images of the PTEN-knockdown PC12 cells, which were transfected with sh-EGFP, or shRNAs for MOB1 (sh-MOB1A or sh-MOB1B), were incubated with anti-NF200 and anti-MOB1. Scale bar, 100 μm (**a**). The quantification of the percentage of cells with neurites showing a significant decrease in a stable PTEN-knockdown PC12 cells transfected with sh-MOB1 groups (*$P < 0.05$ vs. sh-PTEN group, ANOVA test followed by Dunnett's post hoc test) (**b**). **c**, **d** Western blot analysis showing protein bands on the gel for the stable PTEN-knockdown PC12 cells transfected with sh-EGFP or shRNAs for MOB1 (sh-MOB1A or sh-MOB1B), respectively. There were significant differences in neural protein expression (*$P < 0.05$ vs. sh-PTEN group, #$P < 0.05$ vs. sh-EGFP group, ANOVA test followed by Dunnett's post hoc test). **e** Cytoplasmic and nuclear fractions were prepared from sh-EGFP or sh-PTEN-transfected PC12 cells. p-YAP and YAP protein levels were determined by western blot. β-Tubulin and histone served as internal controls. **f**–**h** sh-EGFP or sh-PTEN plasmids were transfected into PC12 and NIH3T3 cells for 48 h, respectively. Lysates were immunoblotted with anti-PTEN, anti-MOB1, anti-p-YAP (S127), anti-YAP and anti-GAPDH antibodies. GAPDH served as an internal control (*$P < 0.05$, *t* test)

(Fig. 5i–k). Overexpression of GSK3β inhibited MOB1 upregulation and decreased neurite outgrowth-related protein expression in PTEN knockdown cells (Fig. 5l, m). Taken together, these results indicated that GSK3β kinase regulates the degradation of the MOB1 protein.

GSK3β interacts with MOB1 and regulates its ubiquitination

To investigate whether GSK3β interacts with MOB1, we used mouse fibroblast NIH3T3 cell lines as in vitro research models for this study. As shown in Fig. 6a, GSK3β was present in MOB1 immunoprecipitates, but not in normal rabbit IgG precipitates. We also found that exogenous MOB1A and MOB1B with Flag-tagged pulled down endogenous GSK3β and Flag-GSK3β interacted with endogenous MOB1 (Fig. 6b–d). Previous studies showed that MOB1 was ubiquitylated and degraded by praja2 in glioblastoma [44]. Here, we tested whether MOB1 was degraded by ubiquitin proteasome system in mouse cells. As shown in Fig. 6e, MOB1 formed a high ubiquitin state in NIH3T3 cells treated with MG132 for 4 h. From the findings above, we postulated that GSK3β promotes MOB1 degradation through the ubiquitin proteolytic pathway. Accordingly, treatment with the proteasome inhibitor MG132 reversed the GSK3β-induced decrease in levels of endogenous MOB1 (Fig. 6f, g). Finally, we constructed GSK3β shRNA and found that GSK3β knockdown increased the expression of MOB1, and that MOB1 had a weak ubiquitination when co-expressed with GSK3β shRNA, indicating that MOB1 protein was ubiquitinated in a GSK3β-dependent manner (Fig. 6h–k).

To confirm the results above, direct interaction between GSK3β and MOB1 was detected by IP assays and double immunofluorescence staining in primary hippocampal neurons. As shown in Figure S2f, GSK3β was present in MOB1 immunoprecipitates, but not in normal rabbit IgG precipitates. Additionally, double immunofluorescence staining (GSK3β and MOB1) also confirmed the direct interaction between GSK3β and MOB1 (Figure S1k).

GSK3β phosphorylates MOB1 protein at the Ser146 site and promotes its proteolysis

It has been reported that the classic GSK3β consensus motif is (S/T–X–X–X–S/T) where X is any amino acid. The potential GSK3β phosphorylation sites are the underlined S/T [45, 46]. Analysis of the MOB1 coding sequence identified three motifs that resemble the GSK3β target sequence: T76–XXX–T80, T130–XXX–S134, and S146–XXX–T150 (Fig. 7a). To determine the role of these putative sites in MOB1 protein stability, we generated T76A, T130A, and S146A mutants by mutating the serine or threonine at the sites of Flag-MOB1A plasmid to alanine and transferred them into NIH3T3 cells treated with CHX for the indicated times. The S146A mutant had a significantly longer half-life than wild type (WT), while T76A and T130A mutants were not significantly changed (Fig. 7b, c). Consistent with its longer half-life, the S146A mutant was less bound to GSK3β compared to MOB1 WT and had the lowest ubiquitination level among the MOB1 mutants and WT (Fig. 7d, e). Given that the S146A mutant of MOB1 cannot be phosphorylated by GSK3β, we tested whether it could block the GSK3β-induced inhibition of neurite outgrowth. Indeed, as shown in Fig. 7f, g, exogenous GSK3β degraded MOB1 WT and mutants, but not S146A, to inhibit NF200 expression in PC12 cells. However, overexpression of S146A mutant plasmids alone did not significantly increase the length of neurites or expression levels of neurite markers (NF200, GAP43, p-GAP43) compared with MOB1 WT and T76A mutant (Fig. 7h–k). Together, these results strongly suggest that PTEN–GSK3β axis phosphorylates MOB1 at Ser146 site and promotes its ubiquitination to inhibit neurite outgrowth in vitro (Fig. 7l).

PTEN-regulated MOB1 expression affects the neurite outgrowth, formation of glial scar and functional recovery following SCI

The effects of PTEN–GSK3β-regulated MOB1 expression on neurite outgrowth in vitro suggest the physiological significance of the PTEN–MOB1 axis in the contusion model of SCI. Therefore, we investigated the impact of MOB1 silencing on neurite outgrowth and functional recovery after SCI in the context of PTEN inhibition. After SCI in mice, we injected lentivirus shRNA vectors targeted at PTEN

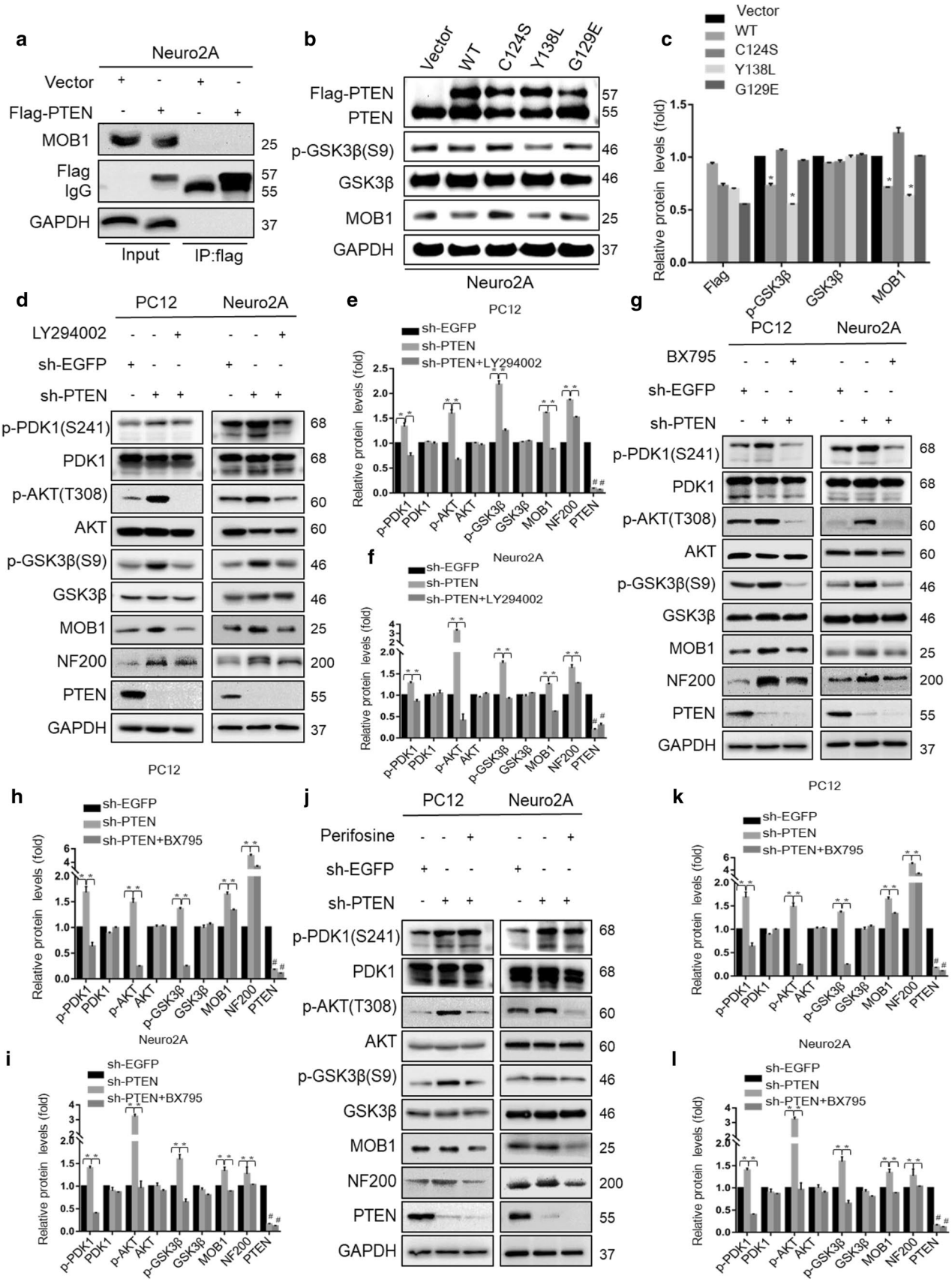
a
Neuro2A
Vector + - + -
Flag-PTEN - + - +
MOB1
Flag IgG
GAPDH
25
57 55
37
Input IP:flag
b
Vector WT C124S Y138L G129E
Flag-PTEN
PTEN
p-GSK3β(S9)
GSK3β
MOB1
GAPDH
57 55
46
46
25
37
Neuro2A
c
Vector
WT
C124S
Y138L
G129E
Relative protein levels (fold)
Flag
p-GSK3β
GSK3β
MOB1
d
PC12 Neuro2A
LY294002 - - + - - +
sh-EGFP + - - + - -
sh-PTEN - + + - + +
p-PDK1(S241)
PDK1
p-AKT(T308)
AKT
p-GSK3β(S9)
GSK3β
MOB1
NF200
PTEN
GAPDH
68 68 60 60 46 46 25 200 55 37
PC12
e
PC12
sh-EGFP
sh-PTEN
sh-PTEN+LY294002
Relative protein levels (fold)
p-PDK1 PDK1 p-AKT AKT p-GSK3β GSK3β MOB1 NF200 PTEN
f
Neuro2A
sh-EGFP
sh-PTEN
sh-PTEN+LY294002
Relative protein levels (fold)
p-PDK1 PDK1 p-AKT AKT p-GSK3β GSK3β MOB1 NF200 PTEN
g
PC12 Neuro2A
BX795 - - + - - +
sh-EGFP + - - + - -
sh-PTEN - + + - + +
p-PDK1(S241)
PDK1
p-AKT(T308)
AKT
p-GSK3β(S9)
GSK3β
MOB1
NF200
PTEN
GAPDH
68 68 60 60 46 46 25 200 55 37
PC12
h
sh-EGFP
sh-PTEN
sh-PTEN+BX795
Relative protein levels (fold)
p-PDK1 PDK1 p-AKT AKT p-GSK3β GSK3β MOB1 NF200 PTEN
Neuro2A
i
sh-EGFP
sh-PTEN
sh-PTEN+BX795
Relative protein levels (fold)
p-PDK1 PDK1 p-AKT AKT p-GSK3β GSK3β MOB1 NF200 PTEN
j
PC12 Neuro2A
Perifosine - - + - - +
sh-EGFP + - - + - -
sh-PTEN - + + - + +
p-PDK1(S241)
PDK1
p-AKT(T308)
AKT
p-GSK3β(S9)
GSK3β
MOB1
NF200
PTEN
GAPDH
68 68 60 60 46 46 25 200 55 37
k
sh-EGFP
sh-PTEN
sh-PTEN+BX795
Relative protein levels (fold)
p-PDK1 PDK1 p-AKT AKT p-GSK3β GSK3β MOB1 NF200 PTEN
Neuro2A
l
sh-EGFP
sh-PTEN
sh-PTEN+BX795
Relative protein levels (fold)
p-PDK1 PDK1 p-AKT AKT p-GSK3β GSK3β MOB1 NF200 PTEN

◂**Fig. 4** Lipid phosphatase activity of PTEN regulates MOB1 protein level in vitro. **a** Neuro2A cells were transfected with Flag-PTEN or vector constructs. After 48 h of transfection, cells were lysed and 5% of lysate was used as input control and the remaining lysate was subjected to IP with an anti-Flag antibody. Input and IP were analyzed by western blotting. **b**, **c** Immunoblotting (IB) of PTEN, p-GSK3β (S9), GSK3β and MOB1 in Neuro2A cells transduced with WT or mutant PTEN (C124S, Y138L, or G129E). GAPDH was used as a loading control (*$P<0.05$ vs. sh-PTEN group, #$P<0.05$ vs. sh-EGFP group, ANOVA test followed by Dunnett's post hoc test). **d**–**l** Stable PTEN-knockdown PC12 and Neuro2A cells were treated with specific pharmacological inhibitors of PTEN-PI3K downstream pathways for 2 h: 20 μM LY294002 (PI3K inhibitor) (**d**–**f**), 2 μM BX795 (PDK1 inhibitor) (**g**–**i**) and 20 μM Perifosine (Akt inhibitor) (**j**–**l**). Levels of p-PDK1 (S241), PDK1, p-Akt (T308), Akt, p-GSK3β (S9), GSK3β, MOB1,NF200 and PTEN were determined by IB. GAPDH served as an internal control (*$P<0.05$ vs. sh-PTEN group, #$P<0.05$ vs. sh-EGFP group, ANOVA test followed by Dunnett's post hoc test)

and MOB1 into the injured spinal cord of mice and waited 6 weeks.

One week after SCI, spinal cord sections processed for H&E staining showed similar lesion size, independently of the SCI group (Figure S2a and b). Meanwhile, the relative expression of PTEN and MOB1 was measured after SCI by western blot and the results revealed that the Lenti-shRNA sequences and patterns were useful (Figure S2c and d). Subsequently, the functional recovery of the SCI mice was evaluated. As shown in Fig. 8a, the mice BMS scores were 9 points in all four groups before injury. Immediately after SCI, all mice demonstrated significant loss of motor function of the hind limbs and the BMS scores were reduced to 0. Thereafter, the BMS score increased gradually in all mice, and reached 6.25 ± 0.43 in the Lenti-sh-PTEN group at 6 weeks after injury, which meant that the hind limbs showed frequent or consistent plantar stepping, coordination, and paws parallel at initial contact. On the contrary, the BMS scores at the same time point in the Lenti-eGFP and Lenti-sh-PTEN + Lenti-sh-MOB1 groups were 3.8 ± 0.74 and 4 ± 0.89, respectively. After 2 weeks post-injury, the BMS scores increased significantly in the Lenti-sh-PTEN group compared with the other two SCI groups. We then performed a footprint test by evaluating weight-supported plantar stepping 6 weeks after SCI. Based on the recovery levels and BMS scores in control SCI, we could not measure the footprint distance consistently because the animals dragged their legs. However, the pictures showed that the motor function of the hind limbs in the Lenti-sh-PTEN group was significantly improved compared with other two SCI groups (Fig. 8b).

To explore the role of PTEN and MOB1 inactivation in neurons in vivo, NF200, a neurofilament protein and a marker of neurites/neurons, was used to mark neurons. Microscopy images showed that the positive response area of NF200 staining (in the rostral, caudal and central parts of the lesion) in the Lenti-sh-PTEN group was the largest and the length of neurite outgrowth was significantly increased at 6 weeks after injury, compared with the other SCI groups (Fig. 8c–f). In addition, we measured the glial scars by immunofluorescence staining (GFAP) and carried out a quantitative analysis. The results showed that PTEN inhibition promoted the formation of the glial scar after SCI, and this effect was reversed by down-regulation of MOB1 (Figure S2e and f). The expression of MOB1 in different nerve cells at 4 weeks after SCI was analyzed by double immunofluorescence staining. The results showed that MOB1 expression was higher in neurons (NeuN) and astrocytes (GFAP), compared to oligodendrocytes (OLIG2) (Figure S2g), indicating that the PTEN–MOB1 axis may also regulate the formation of a glial scar. In line with these results, shRNA against PTEN promoted neurite outgrowth and functional recovery in spinal cord contusion mice. This phenomenon was reversed by MOB1 knockdown.

Discussion

In this study, we have revealed for the first time that MOB1, a key node of the PTEN–GSK3β axis, regulates neurite outgrowth and functional recovery after SCI in mice. Specifically, we demonstrate that GSK3β modulates the phosphorylation of MOB1 at serine 146 (which is a direct substrate of GSK3β) and promotes its proteolysis by the UPS in vitro. Therefore, the PTEN–GSK3β-induced proteolysis of MOB1 represents a novel mechanism for controlling neurite outgrowth and functional recovery after SCI.

MOB1, a microtubule-associated protein, plays a critical role in the neurite outgrowth. Previous studies have shown that microtubules are the principal cytoskeletal components of neurites and axons, and control of microtubule assembly is a key regulatory step in neurite outgrowth during regeneration after SCI [21]. MOB1 is involved in the centrosome duplication [6] and microtubule stability [8]. The kinases NDR1/2 are direct downstream targets of MOB1 that promote neurite sprouting during the spinal cord development process [12, 47]. In this study, we found that MOB1 was involved in the development of mice brain and spinal cord, because overexpression of MOB1 significantly promoted neurite outgrowth in neuronal cell models and primary hippocampal neurons. These results provide direct evidence that MOB1 contributes to neurite outgrowth in mammalian CNS. Although previous studies found that up-regulation of MOB1 in Neuro2A cells did not promote neurite formation [13], it is likely that the high level of endogenous MOB1 expression in Neuro2A cells suppresses the acute effects (36 h) of exogenous MOB1.

The PTEN–MOB1 axis controls neurite outgrowth and functional recovery after SCI. Many studies have reported that inactivation of PTEN by various approaches promotes

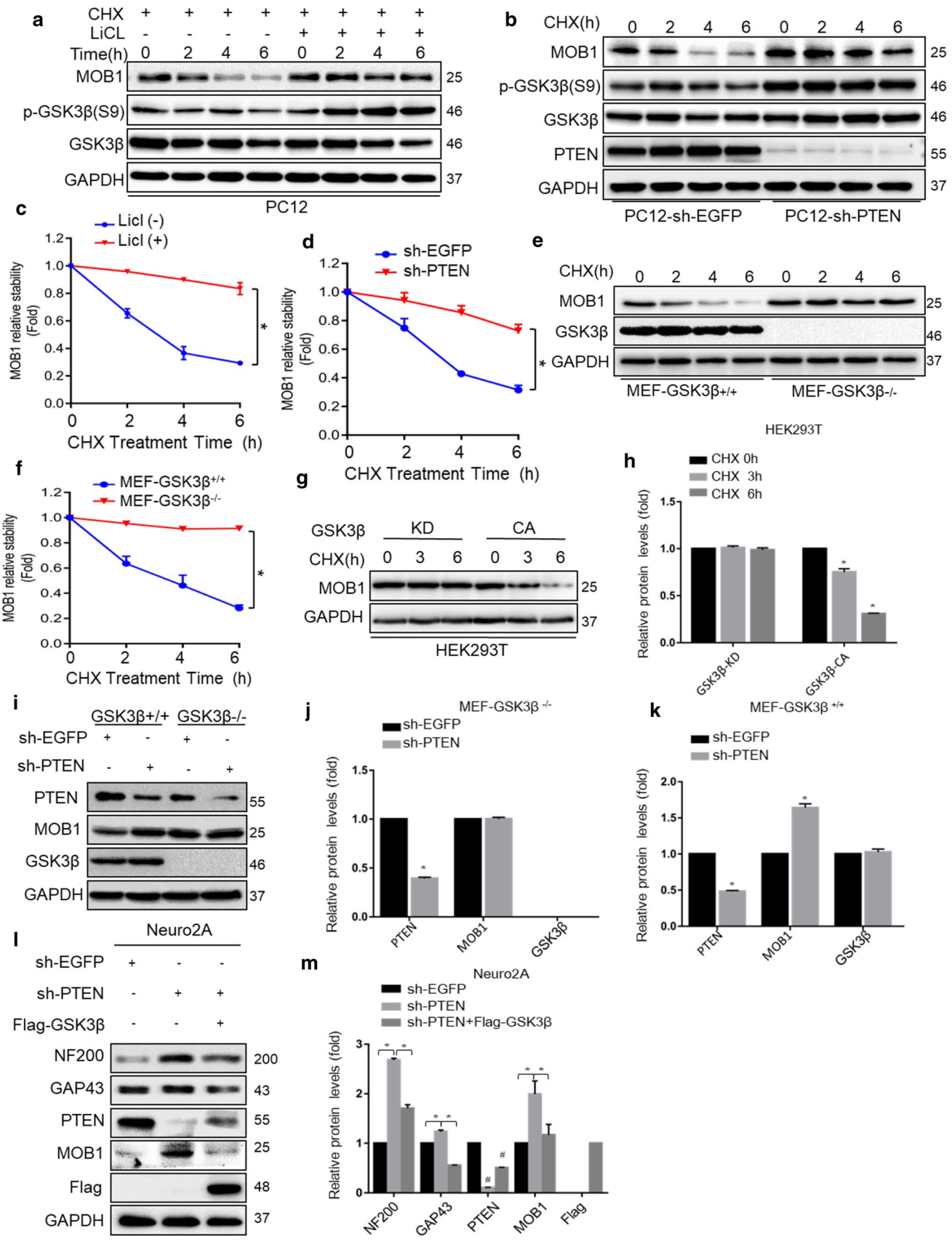
a
CHX
LiCL
Time(h)
MOB1
p-GSK3β(S9)
GSK3β
GAPDH
PC12
b
CHX(h)
MOB1
p-GSK3β(S9)
GSK3β
PTEN
GAPDH
PC12-sh-EGFP
PC12-sh-PTEN
c
Licl (-)
Licl (+)
MOB1 relative stability (Fold)
CHX Treatment Time (h)
d
sh-EGFP
sh-PTEN
MOB1 relative stability (Fold)
CHX Treatment Time (h)
e
CHX(h)
MOB1
GSK3β
GAPDH
MEF-GSK3β+/+
MEF-GSK3β-/-
f
MEF-GSK3β+/+
MEF-GSK3β-/-
MOB1 relative stability (Fold)
CHX Treatment Time (h)
g
GSK3β
KD
CA
CHX(h)
MOB1
GAPDH
HEK293T
h
HEK293T
CHX 0h
CHX 3h
CHX 6h
Relative protein levels (fold)
GSK3β-KD
GSK3β-CA
i
GSK3β+/+
GSK3β-/-
sh-EGFP
sh-PTEN
PTEN
MOB1
GSK3β
GAPDH
j
MEF-GSK3β -/-
sh-EGFP
sh-PTEN
Relative protein levels (fold)
PTEN
MOB1
GSK3β
k
MEF-GSK3β +/+
sh-EGFP
sh-PTEN
Relative protein levels (fold)
PTEN
MOB1
GSK3β
l
Neuro2A
sh-EGFP
sh-PTEN
Flag-GSK3β
NF200
GAP43
PTEN
MOB1
Flag
GAPDH
m
Neuro2A
sh-EGFP
sh-PTEN
sh-PTEN+Flag-GSK3β
Relative protein levels (fold)
NF200
GAP43
PTEN
MOB1
Flag

◂**Fig. 5** GSK3β kinase regulates the stability of the MOB1 protein. **a**, **c** MOB1 expression level was determined in PC12 cells treated with or without GSK3β inhibitor LiCl (20 mM) and CHX (10 μM) for indicated time points (0, 2, 4 and 6 h) (**a**). GAPDH served as an internal control. The quantification of densitometry levels of MOB1 (*$P<0.05$, ANOVA test) (**c**) GAPDH was used as a loading control. MOB1 expression level was determined in PC12-sh-PTEN cells and PC12-sh-EGFP cells treated with CHX for indicated time points (**b**). GAPDH served as an internal control. The quantification of densitometry levels of MOB1 (*$P<0.05$, ANOVA test) (**d**). GSK3β wild-type (WT) and knockout (KO) cells were treated with CHX (10 μM) for the indicated times, and MOB1 and GSK3β expression levels were determined by western blotting (**e**). GAPDH served as an internal control. The quantification of densitometry levels of MOB1 (*$P<0.05$, ANOVA test) (**f**). GSK3β-CA or GSK3β-KD plasmids were transfected into HEK293T cells for 48 h. The cells were then treated with CHX (10 μM) for the indicated times. Endogenous MOB1 expression level was determined by western blotting. GAPDH served as an internal control (**g**). GAPDH served as an internal control. The quantification of densitometry levels of MOB1 protein (*$P<0.05$, ANOVA test) (**h**). **i–k** Knockdown of PTEN did not increase MOB1 expression in MEF GSK3β$^{-/-}$ cells. Protein expression was analyzed by western blotting. GAPDH served as an internal control (*$P<0.05$, *t* test). **l**, **m** Stable PTEN-knockdown Neuro2A cells were transfected with Flag-GSK3β. Protein expression was analyzed by western blotting. GAPDH served as an internal control (*$P<0.05$ vs. sh-PTEN group, $^{\#}P<0.05$ vs. sh-EGFP group, ANOVA test followed by Dunnett's post hoc test)

different degrees of neurite outgrowth in CNS injuries [15, 48, 49], up-regulation of the PI3K/Akt signaling pathway and its downstream effectors, such as mTOR and GSK3β [18, 50, 51]. In our previous study, we showed that expression of various components of the PI3K/Akt signaling pathway altered during SCI in mice [52]. Consistently, this study found that suppression of PTEN enhanced neurite outgrowth via activation of the PI3K/Akt/GSK3β pathway. Importantly, we show, for the first time, a direct mechanistic link between MOB1 protein and PTEN–GSK3β axis in regulating neurite outgrowth. We found that PTEN knockdown significantly up-regulated MOB1 protein expression in primary hippocampal neurons and down-regulation of MOB1 blocked PTEN sh-RNA-induced neurite outgrowth and functional recovery after SCI in mice, suggesting that MOB1 is a key effector of PTEN–GSK3β axis-mediated neurite outgrowth in the injured CNS [53]. Previous study demonstrated that conditional genetic deletion of PTEN enhanced regenerative growth of CST axons, and on cross sections axons extended into and around the lesion with exuberant axon arborization ventrally in the gray matter below the lesion [54]. In this study, PTEN–MOB1 axis regulation of motor function recovery in mice could be partly attributed to sprouting of spared and injured axons, rostral and caudal to the lesion. However, on cross sections, it will be further addressed whether there is an enhanced sprouting within the ventral area, or an evenly distributed NF200-immunoreactivity.

Recent studies found that deletion of PTEN or inhibition with bisperoxovanadium (bpV) constitutively activated the Akt/mTOR signaling, thereby, producing neuroprotective effects in CNS injury/disease [55–57]. Considering that the increased NF-200 immunoreactivity was observed at relatively early time after injury, we speculate that Lenti-sh-PTEN may offer additional neuroprotection after SCI. However, it is not clear whether MOB1 is involved in sh-PTEN-induced neuroprotective effects after SCI.

It is noteworthy that PTEN–MOB1 axis may be involved in the formation of the glial scar after SCI. Accumulating evidence suggests that PTEN and PI3K/Akt signaling pathway are involved in glial scar formation [53, 58]. Similarly, the results demonstrated that PTEN inhibition promoted the formation of glial scar after SCI, and this effect was reversed by down-regulation of MOB1. Recent studies have suggested that loss of PTEN may promote neural stem cells proliferation and differentiation [59]. On the other hand, MOB1 contributes to stem cell differentiation [60], indicating that the PTEN–MOB1 axis may affect the astrocytes during the differentiation of endogenous neural stem cells in the spinal cord.

Additionally, PTEN–MOB1 axis-mediated neurite outgrowth is independent of the Hippo-YAP pathway. As a positive regulator of the Hippo cascade, MOB1 activates the LATS1/2, which mediates phosphorylation of YAP at Ser127 to inhibit its nuclear localization and transcriptional activity [29, 44]. However, our results showed that PTEN-induced MOB1 degradation did not affect the phosphorylation of YAP or YAP nuclear translocation in vitro, probably because other molecules of the PTEN-PI3K pathway may be involved in regulation of Hippo pathway [61, 62]. Hence, it is important to study the relationship between the PTEN-PI3K and Hippo-YAP pathways to reveal the role of this complex signal transduction network in the recovery of SCI.

MOB1 is a novel substrate for GSK3β that is phosphorylated on serine 146 and degraded via the UPS. Accumulating evidences indicate that GSK3β phosphorylates a broad range of microtubule-interacting proteins to regulate specific aspects of microtubule assembly in axons [63], including CRMP2 [23], MAP1B [64] and tau [64]. For example, GSK3β controls neurite branching and microtubule dynamics by phosphorylating the microtubule-associated protein MAP1B [65]. Yet, the relationship between MOB1 and other microtubule-associated substrates involved in GSK3β-mediated neurite outgrowth remains unclear. Previous studies reported that most signaling pathways require both phosphorylation and ubiquitination for full regulatory control, and ubiquitination is often regulated by phosphorylation [66]. E3 ubiquitin ligase praja2 regulates MOB1 ubiquitin-mediated proteolysis in glioblastoma [44]. Indeed, we found that the GSK3β-induced MOB1 ubiquitin-mediated proteolysis was required for its Ser146 phosphorylation as the S146A mutant blocked GSK3β-induced inhibition of neurite outgrowth. Thus, these findings provide a novel mechanism

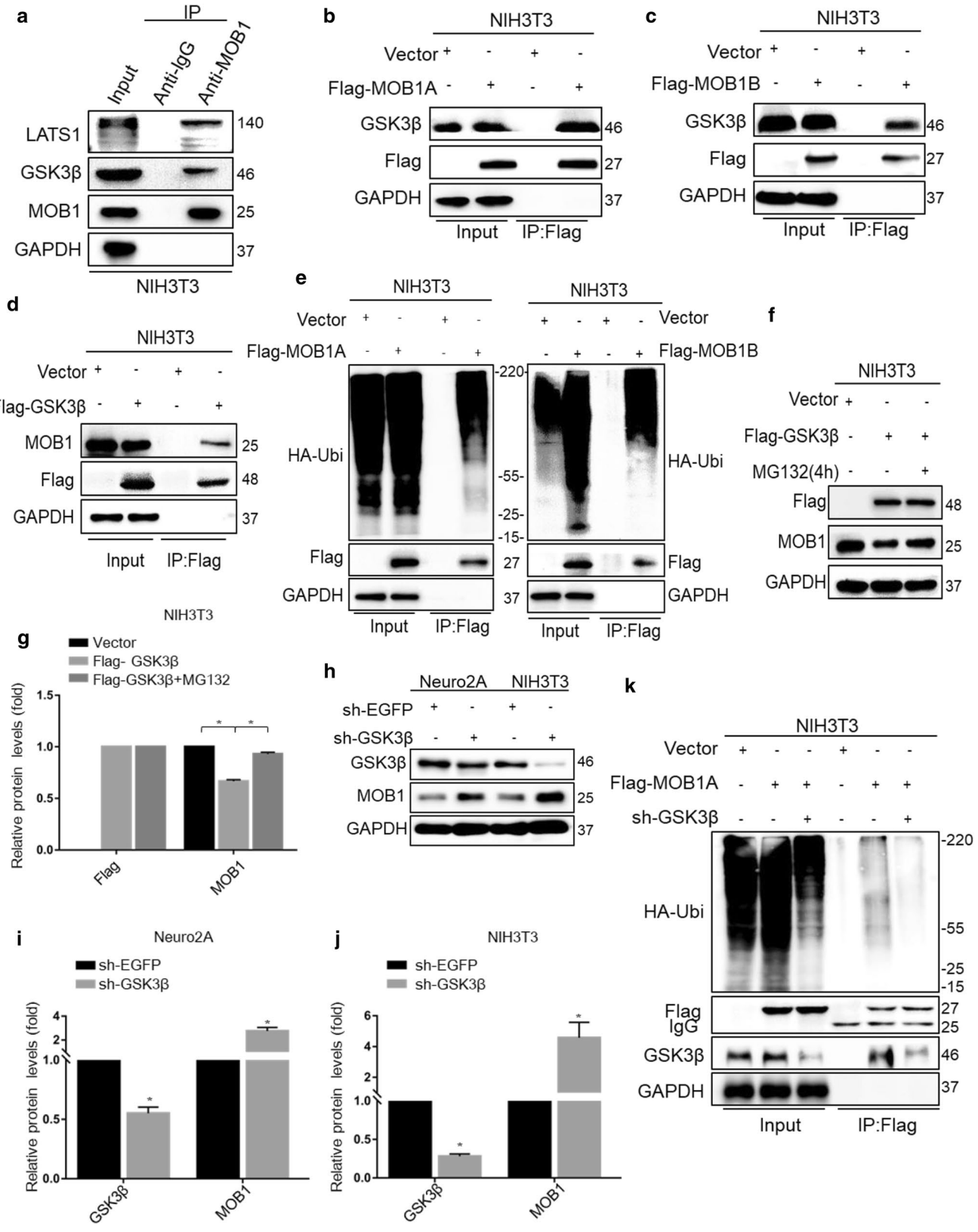
a
IP
Input
Anti-IgG
Anti-MOB1
LATS1
GSK3β
MOB1
GAPDH
140
46
25
37
NIH3T3
b
NIH3T3
Vector
Flag-MOB1A
GSK3β
Flag
GAPDH
46
27
37
Input
IP:Flag
c
NIH3T3
Vector
Flag-MOB1B
GSK3β
Flag
GAPDH
46
27
37
Input
IP:Flag
d
NIH3T3
Vector
Flag-GSK3β
MOB1
Flag
GAPDH
25
48
37
Input
IP:Flag
e
NIH3T3
NIH3T3
Vector
Flag-MOB1A
Vector
Flag-MOB1B
HA-Ubi
Flag
GAPDH
220
55
25
15
27
37
Input
IP:Flag
f
NIH3T3
Vector
Flag-GSK3β
MG132(4h)
Flag
MOB1
GAPDH
48
25
37
g
NIH3T3
Vector
Flag- GSK3β
Flag-GSK3β+MG132
Relative protein levels (fold)
1.5
1.0
0.5
0.0
Flag
MOB1
h
Neuro2A
NIH3T3
sh-EGFP
sh-GSK3β
GSK3β
MOB1
GAPDH
46
25
37
k
NIH3T3
Vector
Flag-MOB1A
sh-GSK3β
HA-Ubi
Flag
IgG
GSK3β
GAPDH
220
55
25
15
27
25
46
37
Input
IP:Flag
i
Neuro2A
sh-EGFP
sh-GSK3β
Relative protein levels (fold)
4
2
1.0
0.5
0.0
GSK3β
MOB1
j
NIH3T3
sh-EGFP
sh-GSK3β
Relative protein levels (fold)
6
4
2
1.0
0.5
0.0
GSK3β
MOB1

◂**Fig. 6** GSK3β interacts with MOB1 and regulates its ubiquitination. **a** Endogenous MOB1 interacts with GSK3β. Cell extracts of NIH3T3 cells were subjected to IP using a MOB1 antibody or control IgG, followed by western blotting with the anti-GSK3β antibody. Lysates were prepared from NIH3T3 cells transfected with the Flag-MOB1A (**b**), Flag-MOB1B (**c**) or Flag-GSK3β (**d**) for 48 h. Lysates were resolved directly by SDS-PAGE or were incubated with anti-Flag antibodies. Precipitates were analyzed by western blotting with the indicated antibodies. **e** Cells were transiently co-transfected with HA-ubiquitin and Flag-MOB1A or Flag-MOB1B. Cells were treated for 4 h with MG132 (20 μM) before harvesting. Lysates were immunoprecipitated with anti-Flag antibody. The precipitates and lysates were immunoblotted with anti-HA, and anti-flag antibodies. **f**, **g** Cells were transiently co-transfected with Vector or Flag-GSK3β plasmids. The cells were treated for 4 h with MG132 (20 μM) before harvesting. Lysates were immunoblotted with the indicated antibodies. GAPDH served as an internal control (*$P < 0.05$ vs. Flag-GSK3β group, ANOVA test followed by Dunnett's post hoc test). **h**, **i** GSK3β knockdown in Neuro2A and NIH3T3 cells increased the expression of MOB1 protein. GAPDH served as an internal control (*$P < 0.05$, *t* test). **k** Flag-MOB1A or vector and sh-EGFP or sh-GSK3β with HA-ubiquitin plasmids were co-transfected into NIH3T3 cells. Cells were treated for 4 h with MG132 (20 μM) before harvesting. Cell lysates were subjected to IP with anti-Flag antibody, followed by IB with anti-HA, anti-Flag and anti-GSK3β antibodies

that adds to our understanding of the roles played by the PTEN–GSK3β–MOB1 axis in neurite outgrowth and functional recovery after SCI.

In addition, it was reported that PTEN is a tumor suppressor and the long-term loss of PTEN might increase susceptibility to cancer conditions or neoplasia in normal tissues [67]. It is possible that suppression of PTEN may lead to abnormal function of its downstream signaling pathways. As a downstream effector of the PTEN–GSK3β axis, MOB1 may be a promising therapeutic target for SCI in contrast to PTEN. Therefore, more studies focusing on the role of MOB1 in neurite outgrowth and identification of a small molecule inhibitor targeting its Ser146 residue are required to drive the discovery of drugs for the treatment of SCI.

In conclusion, this study shows the role of MOB1 in neurite outgrowth and reveals a novel molecular mechanism in which PTEN induces MOB1 degradation to inhibit neurite outgrowth via GSK3β-mediated ubiquitination, which suggests that PTEN–MOB1 axis may be a potential therapeutic target to improve functional recovery after SCI.

Materials and methods

Plasmids and antibodies

Full-length mouse PTEN, MOB1A, MOB1B or GSK3β cDNA was subcloned into the mammalian expression vectors p3xFLAG-CMV-24 (Sigma). Full-length mouse GSK3β cDNA was subcloned into the mammalian expression vectors pcDNA3.1-HA (Sigma, St. Louis, MO, USA). GSK3β-CA, GSK3β-KD and HA-Ubiquitin vectors were provided by University of Jiangsu, Zhenjiang, China. The PTEN-1, PTEN-2, PTEN-3, GSK3β, MOB1A, and MOB1B shRNA oligos (Supplementary Table 1, Sangon Biotech., Shanghai), which had homology between rat and mice cell lines, were first annealed into double strands and then cloned into pLKO.1-puro-vector (Sigma). The primer pairs (Supplementary Table 1) were used to generate the mutation constructs: Flag-PTEN (C124S, Y138L and G129E) and Flag-MOB1A (T76A, T130A and S146A). Point mutations were created using the KOD mutagenesis kit (Toyobo, Osaka, Japan) according to the manufacturer's recommendations.

Antibodies against PTEN (#9188), MOB1 (#13730), p-Akt (#13038), Akt (#4691), p-GSK3β (#9323), GSK3β (#12456), p-PDK1 (#3438), PDK1 (#3062), GAP43 (#8945), NF200 (#2836), LATS1 (#3477), HA-Tag (#3724), Rabbit IgG (#3423), YAP (#14074), p-YAP (#13008) Histone (#9717) β-tubulin (#2128) and GAPDH (#2118) were purchased from Cell Signaling Technology (CST) (Danvers, MA, USA). The antibody against Flag (F1804) was from Sigma. The antibodies against MOB1A (sc-393212) and OLIG2 (sc-293163) antibody were from Santa Cruz Biotechnology (Santa Cruz, CA, USA). The antibody against GFAP (ab10062) and NeuN (ab104224) antibody were from Abcam (Cambridge, MA). The antibody against p-GAP43 (S41) antibody was from Bioworld Technology (St. Louis Park, MN, USA).

Animals

ICR mice from embryonic stage 15 days to 8 weeks were provided by Jiangsu University Animal Experimental Center and maintained in SPF level housing temperature at 21 ± 2 °C, humidity 30–35%, 12/12-h dark/light cycle, with free access to food and water. All experimental procedures were in accordance with the guidelines of animal research of Science and technology department of China, and have been approved by the ethic committee of animal research in Jiangsu University.

Cell culture and treatments

PC12, Neuro2A, HEK293T, and NIH3T3 cells were purchased from the Type Culture Collection of the Chinese Academy of Sciences, Shanghai, China. GL261, BV2, HT22, wild-type and GSK3β double-knockout MEF cells were provided by Jiangsu University. PC12, Neuro2A, BV2, HT22 and GL261 cells were cultured in DMEM/F12 (Hyclone, Beijing, China) with 10% fetal bovine serum (FBS) (Gibco, Carlsbad, CA, USA). Meanwhile, HEK293T, NIH3T3, wild-type and GSK3β double-knockout MEF cells were cultured in DMEM (Hyclone, Beijing, China) containing 10% FBS. All cells were cultured with 1% penicillin/

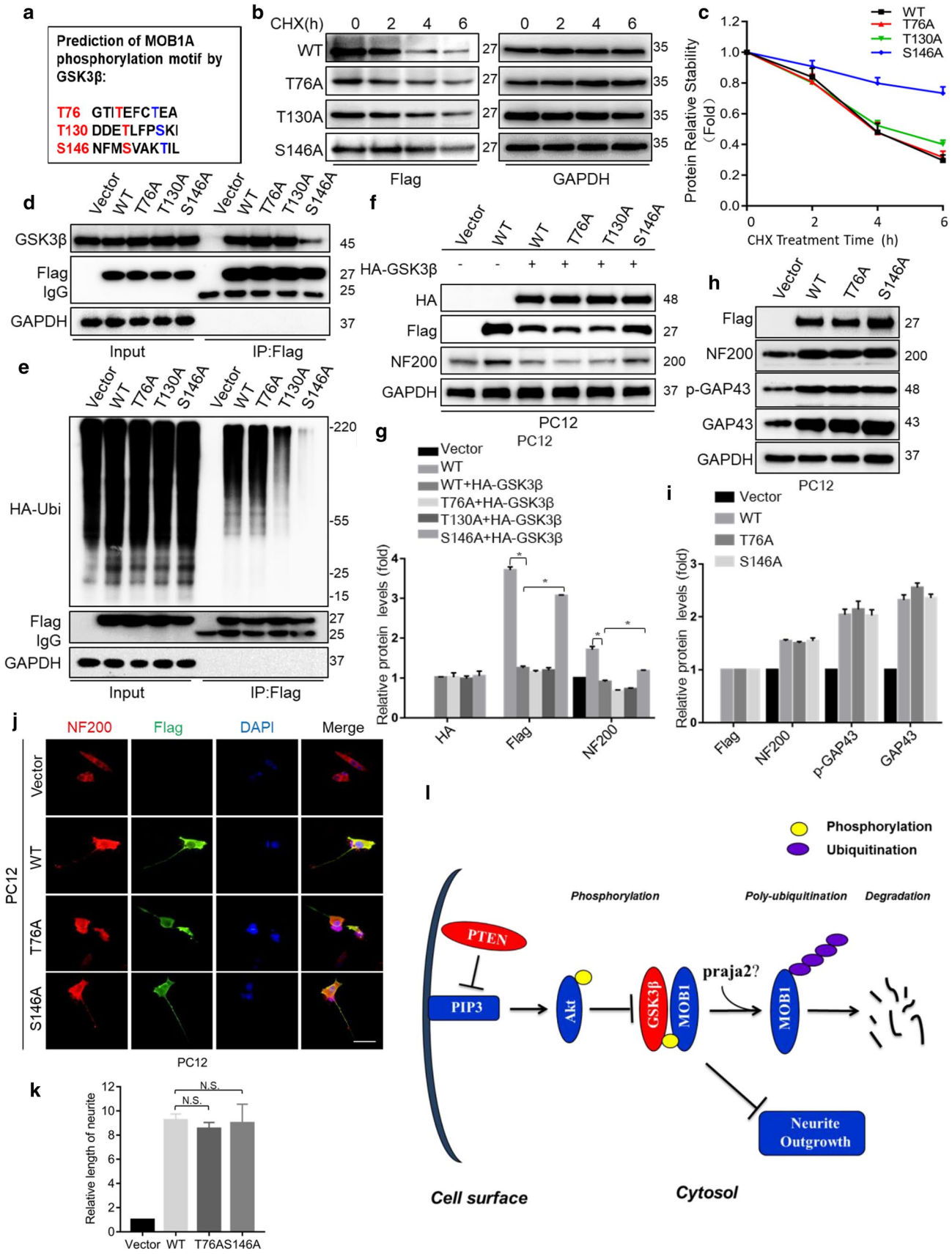
a
Prediction of MOB1A phosphorylation motif by GSK3β:
T76 GTITEFCTEA
T130 DDETLFPSKI
S146 NFMSVAKTIL
b
CHX(h) 0 2 4 6 0 2 4 6
WT
T76A
T130A
S146A
Flag
GAPDH
c
WT
T76A
T130A
S146A
Protein Relative Stability (Fold)
CHX Treatment Time (h)
d
Vector WT T76A T130A S146A Vector WT T76A T130A S146A
GSK3β
Flag IgG
GAPDH
Input
IP:Flag
e
HA-Ubi
Flag IgG
GAPDH
Input
IP:Flag
f
Vector WT WT T76A T130A S146A
HA-GSK3β
HA
Flag
NF200
GAPDH
PC12
g
PC12
Vector
WT
WT+HA-GSK3β
T76A+HA-GSK3β
T130A+HA-GSK3β
S146A+HA-GSK3β
Relative protein levels (fold)
HA
Flag
NF200
h
Vector WT T76A S146A
Flag
NF200
p-GAP43
GAP43
GAPDH
PC12
i
Vector
WT
T76A
S146A
Relative protein levels (fold)
Flag
NF200
p-GAP43
GAP43
j
NF200 Flag DAPI Merge
Vector
WT
T76A
S146A
PC12
k
Relative length of neurite
N.S.
N.S.
Vector WT T76A S146A
l
Phosphorylation
Ubiquitination
Phosphorylation
Poly-ubiquitination
Degradation
PTEN
PIP3
Akt
GSK3β
MOB1
praja2?
MOB1
Neurite Outgrowth
Cell surface
Cytosol

◂**Fig. 7** GSK3β phosphorylates MOB1 protein at the Ser146 site and promotes its proteolysis and working model. **a** Sequence analysis of mouse MOB1A identified three putative GSK3β target sites at T76, T130, and S146. NIH3T3 cells were transfected with Flag-tagged MOB1A (WT) and mutants (T76A, T130A or S146A), respectively. After 48 h, cells were treated with CHX (10 μM) for the indicated time points. Lysates were subjected to IB with Flag antibody and GAPDH served as an internal control (**b**). The curves of MOB1 relative stabilities were shown using the ratio of relative density normalized to that of 0-h group in three independent experiments (**c**). **d** Lysates from NIH3T3 cells expressing MOB1A (WT) or mutants T76A, T130A and S146A were subjected to IP using Flag antibody, followed by IB with GSK3β and Flag antibodies. Vector was used as a control. **e** MOB1A (WT) or mutants T76A, T130A and S146A were co-transfected with HA-Ubiquitin plasmids. Lysates from the above NIH3T3 cells were subjected to IP using Flag antibody, followed by IB with HA and Flag antibodies. Vector was used as a control. **f**, **g** HA-GSK3β and Flag-MOB1A or mutants were co-transfected into PC12 cells. Cell lysates were subjected to IB with anti-HA, anti-Flag, and anti-NF200. GAPDH served as an internal control (*$P < 0.05$ vs. WT group, ANOVA test followed by Dunnett's post hoc test). **h**, **i** Lysates from PC12 cells expressing MOB1A (WT) or mutants T76A and S146A were subjected to IB with Flag, NF200, GAP43 and p-GAP43 antibodies. GAPDH served as an internal control. **j**, **k** Neurite outgrowth in PC12 cells was observed under different conditions. Representative immunofluorescence images of cells treated with anti-NF200 and anti-Flag for PC12 cells transfected with Flag-tagged MOB1A (WT) or mutants (T76A or S146A) are shown. Vector was used as a control. Scale bar, 100 μm (**j**). The quantification of the neurite length in PC12 cells stained with NF200-Cy3 (*N.S.* not significant vs. WT group, ANOVA test followed by Dunnett's post hoc test) (**k**). **l** Working model. PTEN–GSK3β axis promotes ubiquitination and degradation of the MOB1 protein to suppress neurite outgrowth

streptomycin (Thermo Scientific) at 37 °C in a humidified incubator with 5% CO_2 supply. Cells were transfected with the stated constructs in six-well plates or 60-mm dishes using a Lipofectamine 2000 reagent (Invitrogen, Mississauga, ON, Canada). The experimenter was blind to the plasmid transfected in each condition.

Hippocampus were dissected from postnatal 3-d (P 3) mice, digested with papain for 30 min at 37 °C, and dissociated with micropipette tips in Neurobasal-A medium (Gibco) supplemented with 0.5 mM L-glutamine (Sigma) and 2% B27 supplements (Invitrogen). Neurons were then plated onto poly-L-lysine (Sigma)-coated dishes at a density of 150 neurons/mm^2. Neuronal cultures were incubated at 37 °C with 5% CO_2. After neurons attached to poly-L-lysine-coated dishes (24 h after plating), the medium was gently exchanged to new neuronal culturing medium supplemented with 4 μmol Ara-C (Sigma) and 1% penicillin/streptomycin (Thermo Scientific).

Real-time PCR

Total RNA was extracted using RNAiso Plus (Takara, Shiga, Japan). Reverse transcription was performed using RevertAid First-Strand cDNA Synthesis Kit (Thermo, Waltham, MA, USA) according to the manufacturer's specification. Real-time PCR was performed in triplicate in 20 μl reactions with iQ SYBR Premix Ex Taq Perfect Real Time (Bio-Rad Laboratories, Inc., Hercules, CA, USA), 50 ng of first-strand cDNA and 0.2 mg of each primer (Supplementary Table 2). Samples were cycled once at 95 °C for 2 min, and then subjected to 35 cycles of 95, 56, and 72 °C for 30 s each. The expression of each gene was defined from the threshold cycle (C_T) and melting temperatures (T_m) were recorded. The relative mRNA content was calculated using the $2^{-\Delta\Delta C_T}$ method with GAPDH as an endogenous control.

Western blotting and quantitative analysis

Western blot was performed to measure indicated protein levels in cells. The cells were washed with cold PBS before being incubated with RIPA lysis buffer containing protease inhibitor cocktail at 4 °C for 10 min and centrifuged at 4 °C at 12,000*g* for 15 min. The supernatant was removed and the concentration of protein was measured with the BCA method. Proteins (40 μg) were loaded into 8–10% gel and then transferred to the PVDF membrane (EMD Millipore, IPFL00010). The membrane was blocked with 5% non-fat milk for 1 h and then incubated overnight with primary antibodies at 4 °C. The relative band intensity was quantified using the software ImageJ (Version 1.48v, NIH, USA) [68]. Briefly, all protein levels are first normalized to the levels of GAPDH. Then, we would select one of the protein levels as 1 and the rest of the protein levels were compared with it. Separate experiments were conducted three times.

Immunofluorescence on cells

1×10^4 cells were seeded into the 24-well plate. The medium was removed and the cells were washed with cold PBS at 48 h post-transfection. Cells were fixed with 4% paraformaldehyde for 20 min and washed three times with PBST, and permeabilized in 0.3% Triton X-100 for 10 min. After that, the cells were incubated overnight with primary antibodies at 4 °C and then incubated with secondary antibodies for 1 h with the nuclei stained with DAPI for 5–10 min. Pictures were sequentially photographed with fluorescent microscope (Nikon, Tokyo, Japan). To determine the length of neurites extending over the neuronal cell substrate, the longest neurites were measured in micrometer using Image-Pro Plus 6.0 software (Media Cybernetics, Silver Spring, MD, USA). The number of neurites that directly originated from neuronal cell bodies was also calculated.

Immunoprecipitation (IP)

Cells were lysed in IP buffer [10 mM HEPES (pH 8.0), 300 mM NaCl, 0.1 mM EDTA, 20% glycerol, 0.2% NP-40,

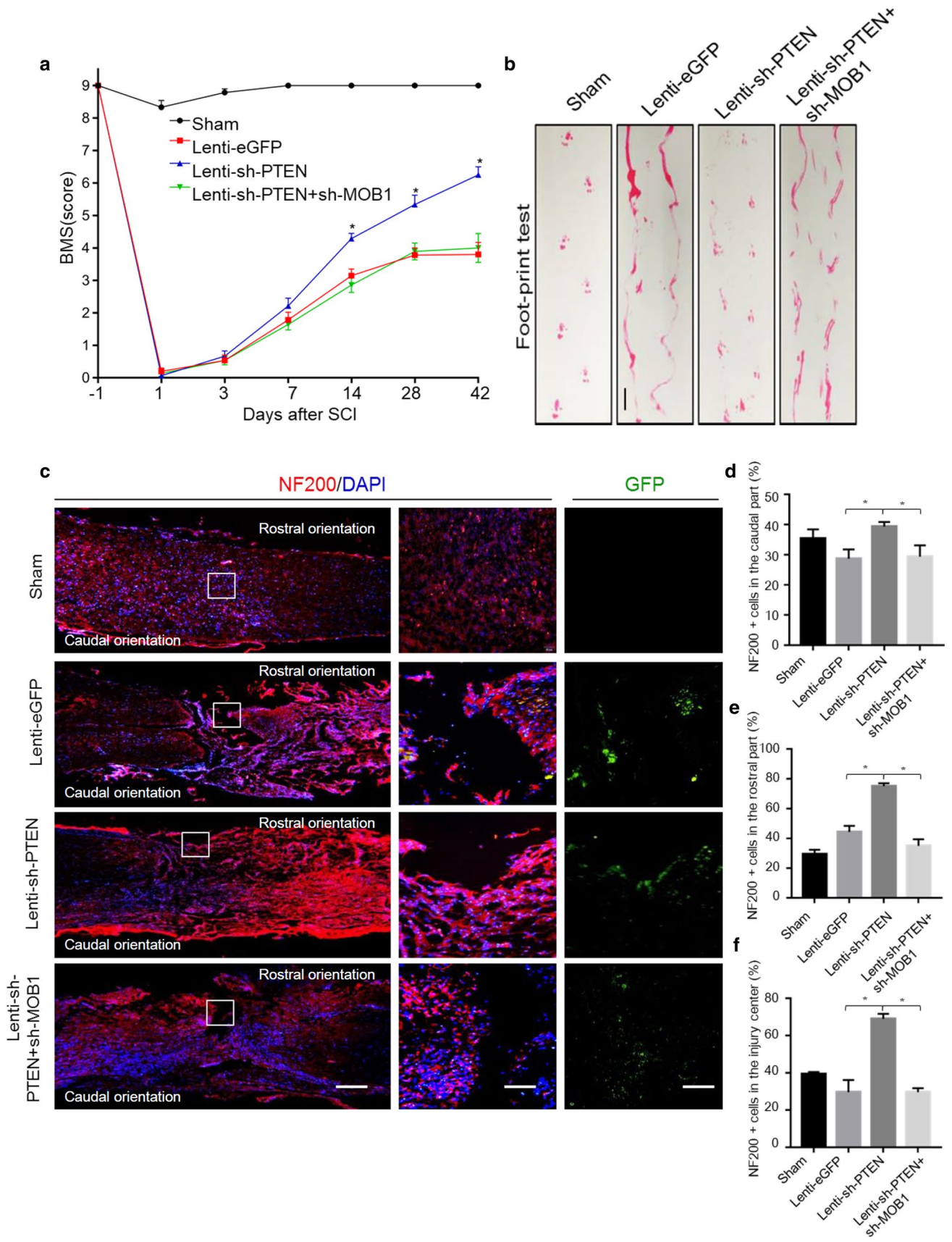
a
BMS(score)
Days after SCI
Sham
Lenti-eGFP
Lenti-sh-PTEN
Lenti-sh-PTEN+sh-MOB1
b
Sham
Lenti-eGFP
Lenti-sh-PTEN
Lenti-sh-PTEN+ sh-MOB1
Foot-print test
c
NF200/DAPI
GFP
Rostral orientation
Caudal orientation
Sham
Lenti-eGFP
Lenti-sh-PTEN
Lenti-sh-PTEN+sh-MOB1
d
NF200 + cells in the caudal part (%)
e
NF200 + cells in the rostral part (%)
f
NF200 + cells in the injury center (%)

◂**Fig. 8** Lentiviral-mediated silencing of MOB1 reverses functional recovery and neurite outgrowth after mouse SCI caused by PTEN knockdown. **a** BMS score was determined before injury (day 1) and at days 1, 3, 7, 14, 28, and 42 after surgery ($n=10$ in Sham group, $n=12$ in Lenti-eGFP group, $n=11$ in Lenti-sh-PTEN group and $n=13$ in Lenti-sh-PTEN + Lenti-sh-MOB1 group). From week 2 following SCI until the end of the experiment, animals of the Lenti-PTEN group consistently exhibited significantly higher BMS scores compared with the two other SCI groups ($^*P<0.05$, two-way repeated measures ANOVA followed by Bonferroni's post hoc test). **b** Footprint data in false-color mode. Four or more consecutive steps were used to determine the mean values of each measurement. Scale bar, 2.5 cm. **c** Representative immunofluorescence images of the longitudinal sections of spinal cord showing NF200-Cy3-labeled neurites in the various groups at 2 weeks after SCI (left panels, lower magnifications, scale bar, 1 mm) (right panels, higher magnifications, scale bar, 100 μm). Quantitative analysis of the $NF200^+$ cells in the rostral (**d**), caudal (**e**) and central (**f**) parts of the spinal cord longitudinal sections, respectively (5–7 mice were used in each group. $^*P<0.05$ vs. Lenti-sh-PTEN group, ANOVA test followed by Dunnett's post hoc test)

protease and phosphatase inhibitors (Thermo Scientific)] and centrifuged under 4 °C at 14,000*g* for 15 min. Five percent of lysate was saved as input control. The remaining lysate was subjected to IP using the first indicated antibodies at 4 °C overnight. Then, the protein complexes were collected by incubation with 30 μl of Protein G-Agarose (Roche, Switzerland) for 2 h at 4 °C. The collected protein complexes were washed six times with co-IP buffer and analyzed by western blotting.

Cytoplasm and nuclear fractionation

Cytoplasm and nuclear fractionation was performed according to the manufacturer's instructions (Vazyme, Nanjing, China). Briefly, cells were washed with cold PBS before being suspended in Isolation buffer A containing protease inhibitor cocktail at 4 °C for 10 min and centrifuged at 4 °C at 12,000*g* for 5 min. The supernatant containing the cytoplasm fraction was collected and stored at − 80 °C. The Isolation buffer B was added to the remaining cell fragments and then rotated for 30 s and repeated four times every 10 min. After 14,000*g* centrifugation at 4 °C for 5 min, supernatant was collected containing the nuclear fractionation and stored at − 80 °C.

Lentivirus packaging and production of stable cell lines

The shRNA sequences targeting mus PTEN and MOB1 (homologous sequence silenced MOB1A together with MOB1B mRNA) are shown in Supplementary Table 2. The backbone vector for shRNA was the GV493 vector (GeneChem, Shanghai, China) and backbone vector for MOB1A was pLenti-CMV-GFP-puro-vector (Public Protein/Plasmid Library, Nanjing, China). The backbone vectors, pHelper 1.0 and pHelper 2.0 packing plasmids (GeneChem) were co-transfected into HEK293T cells using Lipofectamine 2000 (Invitrogen). Supernatant was collected 48 h post-transfection and virus was concentrated by centrifugation (25,000*g* for 2 h at 4 °C). Then the virus was suspended in PBS and frozen at − 80 °C until use. The lentivirus was determined by quantitative real-time PCR. For the determination of infection efficiency, GFP expression in HEK293T cells or spinal cord tissues was analyzed using fluorescence microscope. For target cell transduction, cells were passaged to 40% confluency the following day. Viral medium was added to the cells with Polybrene (8 μg/ml, Sigma). After 24 h, viral particle-containing medium was removed and replaced with fresh medium containing the puromycin (PC12 cells: 8 μg/ml; Neuro2A cells: 1 μg/ml, Sigma). From days 4 to 10, fresh medium was replaced when necessary and evaluated for cytotoxicity under a microscope. Finally, the stable cells were collected for further experiments.

Contusion spinal cord injury surgery and lentiviral vector injection

Female ICR mice aged 6–8 weeks were used in these experiments. Surgical procedures for modeling injury were performed as described previously [52]. Briefly, a laminectomy was performed at T9–T11 levels to expose the T10 thoracic spinal cord, and the spinal cord was contused with a Multicenter Animal Spinal Cord Injury Study (MASCIS) Impactor weight-drop device, which used a 5-g weight impact rod dropped from a height of 25 mm to produce a reliable contused SCI model (impacting force: 125 kdyn). The standard contusion model injury resulted in complete spinal cord injury and loss of motor function of hind limbs in mice. Sham group animals were only subjected to a laminectomy operation without virus injection. Immediately following SCI, the mice were randomized into three groups [Lenti-eGFP (Control shRNA), Lenti-sh-PTEN, and Lenti-sh-PTEN + Lenti-sh-MOB1 (1:1)], and lentiviral vectors were injected into two points at a distance of 1.5 mm rostral and caudal to the center of the injury site with a depth of 1.0 mm. For each site, the mice were injected with 5 μl of lentiviral solution (1×10^8 TU/ml) at a flow rate of 50 μl/min through a glass microinjection needle (0.4 mm in diameter) connected to a Hamilton syringe driven by a microinjection pump. After lentiviral solution delivery, the microinjection needle was left in place for 2 min and then slowly withdrawn from the injection site. Muscles and skin were then sutured. Animals were left to recover and provided with food, sterile water, and the appropriate ambient temperature after the surgery. Meanwhile, tramadol hydrochloride (50 mg/kg body weight) was administered intraperitoneally for the postoperative analgesia. The mice were given manual

bladder evacuations twice per day. The spinal cord located 1 cm proximally and distally to the injury epicenter was removed for serial sagittal/horizontal sections. The serial sections, which were well integrated and close to the injury center, were selected for H&E and fluorescent staining.

Basso mouse scale (BMS) and footprint test

The BMS assesses the locomotion behaviors of mice in an open field. Mice were observed in a blinded manner by two observers for 5 min. Many features were noted, including ankle movements, stepping pattern, coordination, paw placement, trunk instability, and tail position, with a minimum score of 0 (no movement) to a maximum score of 9 (normal locomotion). Mice were tested before injury (day 1) and at days 1, 3, 7, 14, 28, and 42 after SCI. Mice with a BMS score of 3 (some stepping) at 1 day after injury were excluded from the analysis. For footprint test, walking patterns of mouse hind paws were recorded with ink during continuous locomotion across a 50-cm runway, and the stride length on each side and stride width between two sides of the prints were measured and calculated from multiple steps.

Immunofluorescence on tissue

Frozen spinal cord (20 μm thickness) obtained from the injury site and from 1 cm rostral and caudal to the lesion center was used for immunostaining using primary antibodies overnight at 4 °C. Then, sections were incubated with the secondary antibodies labeled with Cy3/FITC at 37 °C for 1 h. The slides were washed with PBS and stained with DAPI and coverslipped using Vectashield mounting media (Vector Laboratories, Burlingame, CA, USA). All samples were processed in parallel under the same condition and observed on a fluorescent microscope (Nikon, Tokyo, Japan). We used five to seven mice in each group, and three sagittal/horizontal sections were serially selected from the medial part of each spinal cord from the animals. Two images were obtained per section from each spinal cord for fluorescent microscopy. Morphological evaluation was quantified using the software ImageJ (Version 1.48v, NIH, USA) [68].

Statistical analysis

All results, expect of animal experiments which are expressed as mean value ± SEM, are expressed as mean value ± SD of three independent experiments ($n = 3$). Differences between experimental groups were evaluated by two-tailed unpaired Student's t test or one-way ANOVA followed by a Dunnett's post hoc test analysis. Repeated measures two-way ANOVA was used to compare matched data at multiple time points, and Bonferroni's post hoc test analysis was used to compare means at each time point unless otherwise stated. $P < 0.05$ was considered to be significant. All statistical analyses were performed using SPSS 18.0 software (IBM Corporation, NY, USA).

Acknowledgements We thank Dawei Wang for his help in some experiments. We also thank Nida Fatima Moazzam (Ph.D.) for her language guidance during the revision of this manuscript. This study was supported by grants from the National Science Foundation of China (81471263), the Natural Science Foundation of Jiangsu Province (BK20151177), Changzhou High-Level Medical Talents Training Project (2016ZCLJ005), the Postdoctoral science foundation of China (2016M600383), and the Special Funded Projects of China Postdoctoral Fund (2017T100337).

Compliance with ethical standards

Conflict of interest All authors declare no competing financial interests.

References

1. Gwak SJ, Macks C, Jeong DU, Kindy M, Lynn M, Webb K, Lee JS (2017) RhoA knockdown by cationic amphiphilic copolymer/siRhoA polyplexes enhances axonal regeneration in rat spinal cord injury model. Biomaterials 121:155–166. https://doi.org/10.1016/j.biomaterials.2017.01.003
2. McDonald JW, Sadowsky C (2002) Spinal-cord injury. Lancet 359(9304):417–425. https://doi.org/10.1016/s0140-6736(02)07603-1
3. Lu Y, Belin S, He Z (2014) Signaling regulations of neuronal regenerative ability. Curr Opin Neurobiol 27:135–142. https://doi.org/10.1016/j.conb.2014.03.007
4. Egawa N, Lok J, Washida K, Arai K (2017) Mechanisms of axonal damage and repair after central nervous system injury. Transl Stroke Res 8(1):14–21. https://doi.org/10.1007/s12975-016-0495-1
5. Luca FC, Winey M (1998) MOB1, an essential yeast gene required for completion of mitosis and maintenance of ploidy. Mol Biol Cell 9(1):29–46
6. Hergovich A, Kohler RS, Schmitz D, Vichalkovski A, Cornils H, Hemmings BA (2009) The MST1 and hMOB1 tumor suppressors control human centrosome duplication by regulating NDR kinase phosphorylation. Curr Biol 19(20):1692
7. Wilmeth LJ, Shrestha S, Montaño G, Rashe J, Shuster CB (2010) Mutual dependence of Mob1 and the chromosomal passenger complex for localization during mitosis. Mol Biol Cell 21(3):380
8. Florindo C, Perdigão J, Fesquet D, Schiebel E, Pines J, Tavares ÁA (2012) Human Mob1 proteins are required for cytokinesis by controlling microtubule stability. J Cell Sci 125(13):3085–3090. https://doi.org/10.1242/jcs.097147
9. Hergovich A (2016) The roles of NDR protein kinases in Hippo signalling. Genes 7(5):21
10. Hergovich A (2011) MOB control: reviewing a conserved family of kinase regulators. Cell Signal 23(9):1433–1440. https://doi.org/10.1016/j.cellsig.2011.04.007
11. Yang R, Kong E, Jin J, Hergovich A, Püschel AW (2014) Rassf5 and Ndr kinases regulate neuronal polarity through Par3 phosphorylation in a novel pathway. J Cell Sci 127(Pt 16):3463
12. Stork O, Zhdanov A, Kudersky A, Yoshikawa T, Obata K, Pape HC (2004) Neuronal functions of the novel serine/threonine kinase Ndr2. J Biol Chem 279(44):45773

13. Lin CH, Hsieh M, Fan SS (2011) The promotion of neurite formation in Neuro2A cells by mouse Mob2 protein. FEBS Lett 585(3):523–530
14. Liu K, Lu Y, Lee JK, Samara R, Willenberg R, Sears-Kraxberger I, Tedeschi A, Park KK, Jin D, Cai B, Xu B, Connolly L, Steward O, Zheng B, He Z (2010) PTEN deletion enhances the regenerative ability of adult corticospinal neurons. Nat Neurosci 13(9):1075–1081. https://doi.org/10.1038/nn.2603
15. Geoffroy CG, Lorenzana AO, Kwan JP, Lin K, Ghassemi O, Ma A, Xu N, Creger D, Liu K, He Z, Zheng B (2015) Effects of PTEN and Nogo codeletion on corticospinal axon sprouting and regeneration in mice. J Neurosci 35(16):6413–6428. https://doi.org/10.1523/JNEUROSCI.4013-14.2015
16. Cantley LC (2002) The phosphoinositide 3-kinase pathway. Science 296(5573):1655–1657. https://doi.org/10.1126/science.296.5573.1655
17. Alessi DR, James SR, Downes CP, Holmes AB, Gaffney PR, Reese CB, Cohen P (1997) Characterization of a 3-phosphoinositide-dependent protein kinase which phosphorylates and activates protein kinase Balpha. Curr Biol 7(4):261
18. Miao L, Yang L, Huang H, Liang F, Ling C, Hu Y (2016) mTORC1 is necessary but mTORC2 and GSK3beta are inhibitory for AKT3-induced axon regeneration in the central nervous system. eLife 5:e14908. https://doi.org/10.7554/elife.14908
19. Zhao T, Qi Y, Li Y, Xu K (2012) PI3 Kinase regulation of neural regeneration and muscle hypertrophy after spinal cord injury. Mol Biol Rep 39(4):3541–3547. https://doi.org/10.1007/s11033-011-1127-1
20. Kim YT, Hur EM, Snider WD, Zhou FQ (2011) Role of GSK3 signaling in neuronal morphogenesis. Front Mol Neurosci 4:48. https://doi.org/10.3389/fnmol.2011.00048
21. Zhou FQ (2005) CELL BIOLOGY: GSK-3 and microtubule assembly in axons. Science 308(5719):211–214. https://doi.org/10.1126/science.1110301
22. Byun J, Kim BT, Kim YT, Jiao Z, Hur EM, Zhou FQ (2012) Slit2 inactivates GSK3beta to signal neurite outgrowth inhibition. PLoS One 7(12):e51895. https://doi.org/10.1371/journal.pone.0051895
23. Liz MA, Mar FM, Santos TE, Pimentel HI, Marques AM, Morgado MM, Vieira S, Sousa VF, Pemble H, Wittmann T, Sutherland C, Woodgett JR, Sousa MM (2014) Neuronal deletion of GSK3beta increases microtubule speed in the growth cone and enhances axon regeneration via CRMP-2 and independently of MAP1B and CLASP2. BMC Biol 12:47. https://doi.org/10.1186/1741-7007-12-47
24. Saijilafu Hur EM, Liu CM, Jiao Z, Xu WL, Zhou FQ (2013) PI3K-GSK3 signalling regulates mammalian axon regeneration by inducing the expression of Smad1. Nat Commun 4(10):2690
25. Li CL, Sathyamurthy A, Oldenborg A, Tank D, Ramanan N (2014) SRF phosphorylation by glycogen synthase kinase-3 promotes axon growth in hippocampal neurons. J Neurosci 34(11):4027–4042. https://doi.org/10.1523/JNEUROSCI.4677-12.2014
26. Gobrecht P, Leibinger M, Andreadaki A, Fischer D (2014) Sustained GSK3 activity markedly facilitates nerve regeneration. Nat Commun 5:4561
27. Di CA, Pesce B, Cordon-Cardo C, Pandolfi PP (1998) Pten is essential for embryonic development and tumour suppression. Nat Genet 19(4):348
28. Lai ZC, Wei X, Shimizu T, Ramos E, Rohrbaugh M, Nikolaidis N, Ho LL, Li Y (2005) Control of cell proliferation and apoptosis by mob as tumor suppressor, mats. Cell 120(5):675–685. https://doi.org/10.1016/j.cell.2004.12.036
29. Ni L, Zheng Y, Hara M, Pan D, Luo X (2015) Structural basis for Mob1-dependent activation of the core Mst-Lats kinase cascade in Hippo signaling. Genes Dev 29(13):1416–1431. https://doi.org/10.1101/gad.264929.115
30. Musatov S, Roberts J, Brooks AI, Pena J, Betchen S, Pfaff DW, Kaplitt MG (2004) Inhibition of neuronal phenotype by PTEN in PC12 cells. Proc Natl Acad Sci USA 101(10):3627–3631. https://doi.org/10.1073/pnas.0308289101
31. Munderloh C, Solis GP, Bodrikov V, Jaeger FA, Wiechers M, Malaga-Trillo E, Stuermer CA (2009) Reggies/flotillins regulate retinal axon regeneration in the zebrafish optic nerve and differentiation of hippocampal and N2a neurons. J Neurosci 29(20):6607–6615. https://doi.org/10.1523/JNEUROSCI.0870-09.2009
32. Benowitz LI, Routtenberg A (1997) GAP-43: an intrinsic determinant of neuronal development and plasticity. Trends Neurosci 20(2):84–91
33. Lin W, Li M, Li Y, Sun X, Li X, Yang F, Huang Y, Wang X (2014) Bone marrow stromal cells promote neurite outgrowth of spinal motor neurons by means of neurotrophic factors in vitro. Neurol Sci 35(3):449–457. https://doi.org/10.1007/s10072-013-1490-x
34. Okumura K, Cavenee WK (2005) Cellular transformation by the MSP58 oncogene is inhibited by its physical interaction with the PTEN tumor suppressor. Proc Natl Acad Offences USA 102(8):2703
35. Tibarewal P, Zilidis G, Spinelli L, Schurch N, Maccario H, Gray A, Perera NM, Davidson L, Barton GJ, Leslie NR (2012) PTEN protein phosphatase activity correlates with control of gene expression and invasion, a tumor-suppressing phenotype, but not with AKT activity. Sci Signal 5(213):ra18
36. Myers MP, Pass I, Batty IH, Kaay JVD, Stolarov JP, Hemmings BA, Wigler MH, Downes CP, Tonks NK (1998) The lipid phosphatase activity of PTEN is critical for its tumor suppressor function. Proc Natl Acad Sci USA 95(23):13513–13518
37. Wu X, Senechal K, Neshat MS, Whang YE, Sawyers CL (1998) The PTEN/MMAC1 tumor suppressor phosphatase functions as a negative regulator of the phosphoinositide 3-kinase/Akt pathway. Proc Natl Acad Sci USA 95(26):15587
38. Vlahos CJ, Matter WF, Hui KY, Brown RF (1994) A specific inhibitor of phosphatidylinositol 3-kinase, 2-(4-morpholinyl)-8-phenyl-4H-1-benzopyran-4-one (LY294002). J Biol Chem 269(7):5241–5248
39. Dangelmaier C, Manne BK, Liverani E, Jin J, Bray P, Kunapuli SP (2014) PDK1 selectively phosphorylates Thr(308) on Akt and contributes to human platelet functional responses. Thromb Haemost 111(3):508–517
40. Gills JJ, Dennis PA (2009) Perifosine: Update on a novel Akt inhibitor. Curr Oncol Rep 11(2):102–110
41. Rubinfeld B, Albert I, Porfiri E, Fiol C, Munemitsu S, Polakis P (1996) Binding of GSK3beta to the APC-beta-catenin complex and regulation of complex assembly. Science 272(5264):1023–1026
42. Kang T, Wei Y, Honaker Y, Yamaguchi H, Appella E, Hung M, PiwnicaWorms H (2008) GSK-3β targets Cdc25A for ubiquitin-mediated proteolysis, and GSK-3β inactivation correlates with Cdc25A overproduction in human cancers. Cancer Cell 13(1):36–47
43. Chen Y, Li Y, Xue J, Gong A, Yu G, Zhou A, Lin K, Zhang S, Zhang N, Gottardi CJ, Huang S (2016) Wnt-induced deubiquitination FoxM1 ensures nucleus beta-catenin transactivation. EMBO J 35(6):668–684. https://doi.org/10.15252/embj.201592810
44. Lignitto L, Arcella A, Sepe M, Rinaldi L, Delle Donne R, Gallo A, Stefan E, Bachmann VA, Oliva MA, Tiziana Storlazzi C, L'Abbate A, Brunetti A, Gargiulo S, Gramanzini M, Insabato L, Garbi C, Gottesman ME, Feliciello A (2013) Proteolysis of MOB1 by the ubiquitin ligase praja2 attenuates Hippo signalling and supports glioblastoma growth. Nat Commun 4:1822. https://doi.org/10.1038/ncomms2791
45. Frame S, Cohen P (2001) GSK3 takes centre stage more than 20 years after its discovery. Biochem J 359:1–16. https://doi.org/10.1042/0264-6021:3590001

46. Doble BW, Woodgett JR (2003) GSK-3: tricks of the trade for a multi-tasking kinase. J Cell Sci 116(7):1175–1186
47. Ultanir SK, Hertz NT, Li G, Ge WP, Burlingame AL, Pleasure SJ, Shokat KM, Jan LY, Jan YN (2012) Chemical genetic identification of NDR1/2 kinase substrates AAK1 and Rabin8 uncovers their roles in controlling dendrite arborization and spine development. Neuron 73(6):1127–1142
48. Ohtake Y, Hayat U, Li S (2015) PTEN inhibition and axon regeneration and neural repair. Neural Regen Res 10(9):1363–1368. https://doi.org/10.4103/1673-5374.165496
49. Huang Z, Hu Z, Xie P, Liu Q (2017) Tyrosine-mutated AAV2-mediated shRNA silencing of PTEN promotes axon regeneration of adult optic nerve. PLoS One 12(3):e0174096. https://doi.org/10.1371/journal.pone.0174096
50. Wyatt LA, Filbin MT, Keirstead HS (2014) PTEN inhibition enhances neurite outgrowth in human embryonic stem cell-derived neuronal progenitor cells. J Comp Neurol 522(12):2741
51. Park SJ, Jin ML, An HK, Kim KS, Ko MJ, Kim CM, Choi YW, Lee YC (2015) Emodin induces neurite outgrowth through PI3K/Akt/GSK-3beta-mediated signaling pathways in Neuro2a cells. Neurosci Lett 588:101–107. https://doi.org/10.1016/j.neulet.2015.01.001
52. Ding Y, Song Z, Liu J (2016) Aberrant LncRNA expression profile in a contusion spinal cord injury mouse model. Biomed Res Int 2016:9249401. https://doi.org/10.1155/2016/9249401
53. Chen CH, Sung CS, Huang SY, Feng CW, Hung HC, Yang SN, Chen NF, Tai MH, Wen ZH, Chen WF (2016) The role of the PI3K/Akt/mTOR pathway in glial scar formation following spinal cord injury. Exp Neurol 278:27–41
54. Danilov CA, Steward O (2015) Conditional genetic deletion of PTEN after a spinal cord injury enhances regenerative growth of CST axons and motor function recovery in mice. Exp Neurol 266:147–160. https://doi.org/10.1016/j.expneurol.2015.02.012
55. Park KK, Liu K, Hu Y, Kanter JL, He Z (2010) PTEN/mTOR and axon regeneration. Exp Neurol 223(1):45–50. https://doi.org/10.1016/j.expneurol.2009.12.032
56. Walker CL, Walker MJ, Liu NK, Risberg EC, Gao X, Chen J, Xu XM (2012) Systemic bisperoxovanadium activates Akt/mTOR, reduces autophagy, and enhances recovery following cervical spinal cord injury. PLoS One 7(1):e30012
57. Liu NK, Xu XM (2012) Neuroprotection and its molecular mechanism following spinal cord injury. Neural Regen Res 7(26):2051–2062. https://doi.org/10.3969/j.issn.1673-5374.2012.26.007
58. Zhang QG, Wu DN, Han D, Zhang GY (2007) Critical role of PTEN in the coupling between PI3K/Akt and JNK1/2 signaling in ischemic brain injury. FEBS Lett 581(3):495–505
59. Amiri A, Cho W, Zhou J, Birnbaum SG, Sinton CM, Mckay RM, Parada LF (2012) Pten deletion in adult hippocampal neural stem/progenitor cells causes cellular abnormalities and alters neurogenesis. J Neurosci 32(17):5880
60. Otsubo K, Goto H, Nishio M, Kawamura K, Yanagi S, Nishie W, Sasaki T, Maehama T, Nishina H, Mimori K, Nakano T, Shimizu H, Mak TW, Nakao K, Nakanishi Y, Suzuki A (2017) MOB1-YAP1/TAZ-NKX2.1 axis controls bronchioalveolar cell differentiation, adhesion and tumour formation. Oncogene. https://doi.org/10.1038/onc.2017.58
61. Lin Z, Zhou P, von Gise A, Gu F, Ma Q, Chen J, Guo H, van Gorp PR, Wang DZ, Pu WT (2015) Pi3kcb links Hippo-YAP and PI3K-AKT signaling pathways to promote cardiomyocyte proliferation and survival. Circ Res 116(1):35
62. Fan R, Kim NG, Gumbiner BM (2013) Regulation of Hippo pathway by mitogenic growth factors via phosphoinositide 3-kinase and phosphoinositide-dependent kinase-1. Proc Natl Acad Sci USA 110(7):2569–2574. https://doi.org/10.1073/pnas.1216462110
63. Hur EM, Zhou FQ (2010) GSK3 signalling in neural development. Nat Rev Neurosci 11(8):539–551. https://doi.org/10.1038/nrn2870
64. Wagner U, Utton M, Gallo JM, Miller CC (1996) Cellular phosphorylation of tau by GSK-3 beta influences tau binding to microtubules and microtubule organisation. J Cell Sci 109(Pt 6):1537–1543
65. Barnat M, Benassy MN, Vincensini L, Soares S, Fassier C, Propst F, Andrieux A, Von BY, Nothias F (2016) The GSK3-MAP1B pathway controls neurite branching and microtubule dynamics. Mol Cell Neurosci 72:9–21
66. Hunter T (2007) The age of crosstalk: phosphorylation, ubiquitination, and beyond. Mol Cell 28(5):730
67. Duan S, Yuan G, Liu X, Ren R, Li J, Zhang W, Wu J, Xu X, Fu L, Li Y, Yang J, Zhang W, Bai R, Yi F, Suzuki K, Gao H, Esteban CR, Zhang C, Izpisua Belmonte JC, Chen Z, Wang X, Jiang T, Qu J, Tang F, Liu GH (2015) PTEN deficiency reprogrammes human neural stem cells towards a glioblastoma stem cell-like phenotype. Nat Commun 6:10068. https://doi.org/10.1038/ncomms10068
68. Schneider CA, Rasband WS, Eliceiri KW (2012) NIH Image to ImageJ: 25 years of image analysis. Nat Methods 9:671–675